

Final Report

on the research project:

Human-Robot Collaboration: Partial
Supplementary Examination [of Pain
Thresholds] for Their Suitability for Inclusion in
Publications of the DGUV and Standardization

Grant number

FP-0430 (funded by German Social Accident Insurance DGUV)

Project contractor



Fraunhofer IFF, Sandtorstr. 22, 39106 Magdeburg, Germany

Authors

Fraunhofer IFF

Otto von Guericke University Trauma
Surgery Clinic

Dr. Roland Behrens
roland.behrens@iff.fraunhofer.de

Dr. Gerald Pliske, MD
gerald.pliske@med.ovgu.de

Table of contents

1	Introduction	2
2	Objectives and General Conditions	3
3	Method and Materials	9
4	Test Procedure.....	13
5	Results	20
6	Discussion	43
7	References	49

Magdeburg, December 19, 2019

1 Introduction

Collaborative robots are intended for operation in a fenceless environment and proximity to humans. Such a constellation has many advantages for professional liability insurers, especially in terms of improved work conditions and ergonomics, better inclusion of workers with special needs, and long-term employment prospects for workers. Moreover, collaborative robots have great potential to mitigate people's impulse to bypass safety guards since they do not restrict access to their work areas. Supported by the German Social Accident Insurance Institution for the Woodworking and Metalworking Industries (BGHM), the Fraunhofer IFF laid the groundwork for refining the biomechanical limits already published by the German Social Accident Insurance (DGUV) in their information sheet FBHM 080. A second objective was to contribute these limit values to the revision of ISO/TS 15066 technical specifications for the organization of safe use of collaborative robots in industry. The first edition of ISO/TS 15066 still in effect includes a list of biomechanical limits indicating the onset of pain. This list is intended to enable robot users to assess their robots' capability to injure humans. The majority of these limits, however, are provisional since a complete set of verified and reliable limits was unavailable when the ISO committee published ISO/TS 15066.

The Fraunhofer IFF has completed three studies to date, which refine and expand the biomechanical limit values in FBHM 080 and ISO/TS 15066. The objective of each study was to determine pain thresholds for a specific load type and a specific set of body locations. In keeping with ISO/TS 15066, we distinguish between the load types of clamping (quasi-static contact) and impact (transient contact). We finished the final study in October of 2019. The quantity of data suffices to specify a set of verified and reliable limit values for all load types and body locations as specified by FBHM 080 and ISO/TS 15066. This report summarizes the results from all the studies completed and presents the desired set of limits.

2 Objectives and General Conditions

2.1 General Approach and Hypotheses

The general approach of all the studies was to subject volunteers to different clamping and impact loads. In every single test, the load intensity was slowly increased until the subject sensed that the pressure stimulus caused slight pain at the loaded body locations. We defined this point as the onset of pain and designated it as the stopping criteria for all load tests as well.

Data from the literature indicate that individuals' pain thresholds are significantly higher when they are exposed to impact loads than when they are exposed to clamping loads (Yamada et al. 1996; Yamada 1997; Yamada et al. 1997). Hence it follows that the rate of the force has an influence on the pain threshold (Takala 1990; List et al. 1991; Isselee et al. 1997; Sarlani und Greenspan 2002). Other sources show that the pain threshold also depends on the size and shape of the contact area (Bishop 1945; Povse et al. 2010b; Povse et al. 2010a, 2011; Saito und Ikeda 2005). In light of these findings, we decided to determine impact and clamping limits with differently shaped contact bodies (probes). The clear evidence in the literature notwithstanding, we hypothesize:

Hypothesis 1: The shorter the period of the contact is, the higher the pain thresholds are.

In addition to the load type and intensity, the type of contact area also has a significant impact on the stress level a load is expected to produce. FBHM 080 and ISO/TS 15066 therefore distinguish between pressure- and force-based limits for both quasi-static and transient contacts. Pressure-based limits are intended for assessments of the degree of risk from semi-sharp robot surfaces, which are likely to come into contact with humans because of foreseeable misuse, while force-based limits are intended for assessments of the risk from blunt robot surfaces. Based on this we can hypothesize:

Hypothesis 2: The smaller the contact area is, the lower the force-based pain thresholds are.

The pain biomechanics of the human body explains this hypothesized relationship. All signals from the nerve endings sensing pain converge at a certain point in the spinal cord. This point functions similarly to a summing unit which only transfers the signals received when their sum exceeds a certain threshold (Vierck et al. 1997). A few high-magnitude signals or a large number of low-magnitude signals can exceed the threshold. A low number of high-magnitude signals are likely to correspond to peak pressures acting on soft tissue, while a large number of low-magnitude signals are likely to correspond to an external load transmitted to the human body by way of a large contact area. Another explanation is the density of the nociceptive nerve endings, which varies according to the body location (Arthur und Shelly 1959; Lauria et al. 1999; Besne et al. 2002).

Figure 1 visualizes the relationship between pressure and force limits introduced (IFA 2009). A threshold curve represents the maximum permissible contact force as a function of the contact area. Any contact situation falling below this curve is unlikely to cause any severe pain or injury, while any contact above the line most likely will. The first part of the curve is a line starting from

the origin. The line has a constant slope that corresponds to the maximum permissible pressure $\hat{\psi}$. Once the contact area \hat{A} reaches a certain size, the curve saturates to the force limit \hat{F} , meaning the size of the contact area A has no effect on the force limit $F(A)$ from this point onward

$$F(A) = \begin{cases} \hat{\psi}A & A \leq \hat{A} \\ \hat{F} & A > \hat{A} \end{cases} .$$

Since the contact area \hat{A} is unknown at the breaking point, it is necessary to establish whether the robot being analyzed and the contact situation exceed both limits. In order to determine $\hat{\psi}$ and \hat{F} for all load types and body locations, we decided to use two differently shaped contact bodies to apply loads to subjects' body locations in the tests (see Section 3.1.3).

We had two differently operating testing systems available to apply clamping and impact loads. The system used to apply clamping loads was an algometer developed by the Institute for Occupational Safety and Health (IFA of the DGUV; see Section 3.1.1). This same system was also used by the University of Mainz, which was in charge of determining the quasi-static and pressure-based limits of ISO/TS 15066. The second system used to apply impact loads was a pendulum, which is a proprietary development of the Fraunhofer IFF (see Section 3.1.2).

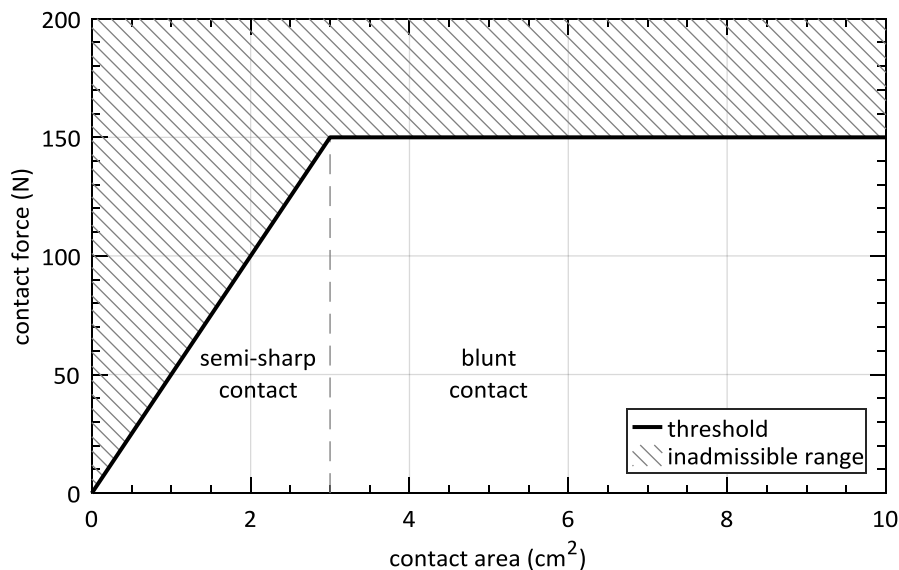


Figure 1. Relationship between pressure and force limits (IFA 2009)

2.2 Partners

The Fraunhofer IFF was in charge of organizing and conducting the studies and analyzed the results obtained. Physicians from Otto von Guericke University Magdeburg's (OvGU)

- Trauma Surgery Clinic,
- Dermatology Clinic,
- Department of Legal Medicine, and
- Neurology Clinic

assisted the Fraunhofer IFF with the studies. They advised the Fraunhofer IFF on all medical issues, represented it at the ethics commission hearings (see Section 2.3.2), and attended the experimental tests. The latter entailed two crucial tasks:

- 1) preparing a report estimating the potential risk of injury for the participating subjects ensuing from the approach followed (see Section 4) to determine the pain threshold using an algometer and a pendulum and
- 2) examining the subjects' health to ensure that none had any preexisting conditions that might put them at risk or potentially distort the results.

2.3 Work Plan

Table 1 presents the work plan of all the studies conducted by the Fraunhofer IFF from 2015 to 2019. It includes the set of body locations tested, the test parameters applied, and the values recorded, all items required by the study. The following examines particular elements of the work plan in more detail and provides an in-depth overview of the scope of all the studies.

Table 1. The work plan of all studies conducted from 2015 to 2019 (nnd. = except all body locations on the dominant hand)

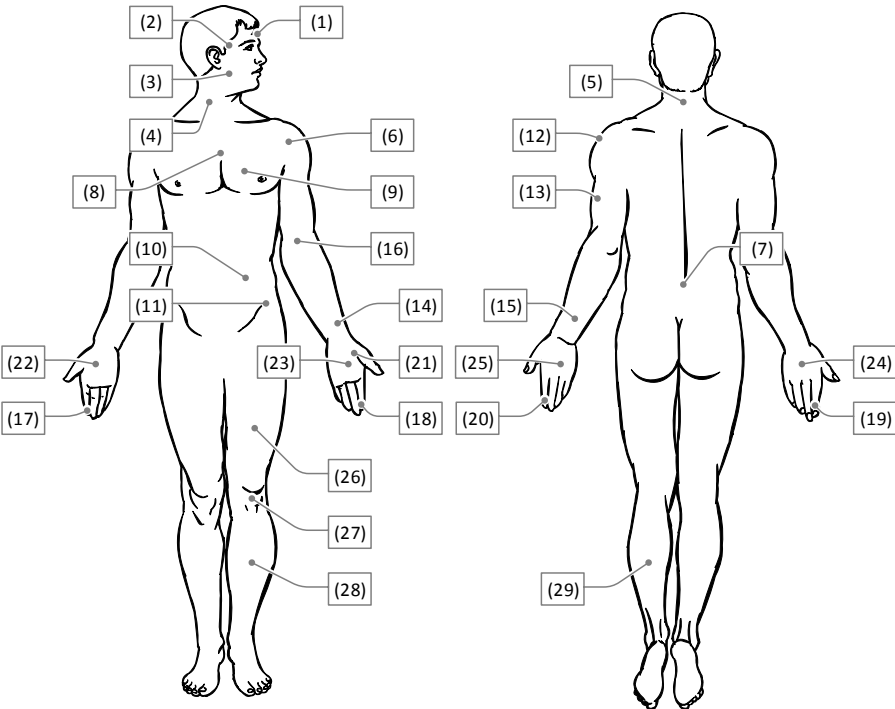
Study no.	1		2		3	
	#1	#2	#3	#4	#4	#5
Subject group size	40	20	20	20	20	10
Body locations (see Figure 2)	(6) ⋮ (29)	(6) (7) ⋮ (11) ⋮ (29)	(6) (7) (11) ⋮ (29)	(1) ⋮ (3) (5)	(1) ⋮ (3) (5) (8) ⋮ (10)	(1) ⋮ (3) (5) ⋮ (29)
Load type						
quasi-static (clamping)	✓			✓		✓
transient (impact)		✓	✓		✓	
Contact body (see Figure 5)						
F-Q10 (pressure limits)		✓	✓		✓	✓
F-Z30 (force limits)	✓	✓	✓	✓	✓	
Impact mass (only for impact tests)						
~6.5 kg		✓	✓		✓	
~16.5 kg		✓	✓		✓	
Repeats	5	1	1	3	1	3
Values measured						
Contact force	✓	✓	✓	✓	✓	✓
Tissue deformation	✓	✓	✓	✓	✓	✓
Contact pressure		(✓)	(✓)		(✓)	✓

2.3.1 Body Locations

Figure 2 presents the body locations, assigning the same identification numbers as used in FBHM 080 and ISO/TS 15066. The names of the body locations on the hand include the suffix D and ND, referring to the dominant (D) and non-dominant (ND) body location. Each body location was pinpointed precisely using a localizing procedure that relies on various anatomical landmarks (see

Appendix 7). This procedure ensured that the load was always precisely applied to the same body location, especially in consecutive tests with subjects.

Prior to the first study, the physicians involved prepared a report in which they assessed the risk to the body locations listed in ISO/TS 15066 ensuing from the load tests. The report specifies a specific order for the testing of all of the body locations in Figure 2 (see Table 2). This order facilitates the gathering of experience with pain-causing loads in tests on body locations (upper and lower extremities) that withstand external loads. The test results indicated that the forces that cause pain are significantly lower than those that can cause severe injuries. This finding made it acceptable to proceed with tests on the rest of the human body in the final study.



Head and neck

- (1) Forehead
- (2) Temple
- (3) Masticatory muscle
- (4) Neck muscle
- (5) 7th Cervical vertebra

Trunk

- (6) Shoulder joint
- (7) 5th lumbar vertebra
- (8) Sternum
- (9) Pectoral muscle
- (10) Abdominal muscle
- (11) Pelvic bone

Upper extremity

- (12) Deltoid muscle
- (13) Humerus
- (14) Radial bone
- (15) Forearm muscle
- (16) Arm nerve

Lower extremity

- (26) Thigh muscle
- (27) Kneecap
- (28) Middle of shin
- (29) Calf muscle

Hand and fingers

- (17) Forefinger pad D
- (18) Forefinger pad ND
- (19) Forefinger end joint D
- (20) Forefinger end joint ND
- (21) Thenar eminence
- (22) Palm D
- (23) Palm ND
- (24) Back of the hand D
- (25) Back of the hand ND

Figure 2. Body locations for which limit values were needed to refine FBHM 080 and ISO/TS 15066

One of the report's distinctive features was its general exclusion of load tests on the neck muscle since the risk of injury from such tests is unacceptably high. Nerve tracts that control vital bodily functions run close to the neck muscles. External loads applied to the neck muscle may be transferred to these tracts and compromise their function. The subject may lose consciousness briefly and suffer a serious fall as a result.

Table 2. Recommended order of testing to mitigate health risks for subjects

		Clamping		Impact		Comments
		1 st	2 nd	1 st	2 nd	
Head and neck	(1) Forehead		✓		✓	
	(2) Temple		✓		✓	
	(3) Masticatory muscle		✓		✓	
	(4) Neck muscle					No tests at all
	(5) 7th Cervical vertebra		✓		✓	
Trunk	(6) Shoulder joint	✓		✓		
	(7) 5th lumbar vertebra	✓		✓		
	(8) Sternum	✓			✓	
	(9) Pectoral muscle	✓			✓	
	(10) Abdominal muscle	✓			✓	
	(11) Pelvic bone	✓		✓		
Upper extremities	(12) Deltoid muscle	✓		✓		
	(13) Humerus	✓		✓		
	(14) Radial bone	✓		✓		
	(15) Forearm muscle	✓		✓		
	(16) Arm nerve	✓		✓		
Hand and fingers	(17) Forefinger pad D	✓		✓		
	(18) Forefinger pad ND	✓		✓		
	(19) Forefinger end joint D	✓		✓		
	(20) Forefinger end joint ND	✓		✓		
	(21) Thenar eminence	✓		✓		
	(22) Palm D	✓		✓		
	(23) Palm ND	✓		✓		
	(24) Back of the hand D	✓		✓		
	(25) Back of the hand ND	✓		✓		
Lower extremities	(26) Thigh muscle	✓		✓		
	(27) Kneecap	✓		✓		
	(28) Middle of shin	✓		✓		
	(29) Calf muscle	✓		✓		

2.3.2 Ethical Approval and Insurance for the Subjects

Otto von Guericke University's ethics committee was in charge of the assessment of the study protocol, its modifications, and the physicians' risk analysis. Ethical approval was granted for all studies, as summarized in Table 3.

The German insurance company HDI insured the subjects against possible injuries resulting from the tests during the studies. Not a single incident required any settlement by the insurer from 2015 to 2019.

Table 3. History of the ethical approval granted by Otto von Guericke University Magdeburg's ethics committee

Date	Study no.	Proposal type	Reference	Proposer
April 27, 2015	1	Full proposal	37/15	Fraunhofer IFF Trauma Surgery Clinic Department of Legal Medicine Neurology Clinic (former Institute for Neuro Radiology) Dermatology Clinic
August 7, 2017	2	Continuation note	37/15	Fraunhofer IFF Trauma Surgery Clinic
February 4, 2019	3	Amendment	13/19	Fraunhofer IFF Trauma Surgery Clinic

3 Method and Materials

3.1 Testing Systems

3.1.1 Algometer for testing quasi-static contacts

We used the algometer pictured in Figure 3 to determine quasi-static limits. This device is designed specifically for this purpose. Our partner IFA supplied the algometer. It is the same as the system used by the University of Mainz, which was in charge of determining quasi-static limits for clamping loads for ISO/TS 15066. The algometer's main component is a mechanism that pushes a rod against a subject's body. A single-axis load inside the pushing mechanism records the contact force applied by the rod.

For reasons of safety, the rod is operated manually by a hand crank. The contact body was mounted on the end of the rod. Linear guides and joints allows the test supervisor to position the loading mechanics perpendicular to any body location specified in the work plan. Various positioning aids such as sockets, vacuum cushions, and straps help keep the body part under test from slipping or shifting.



Figure 3. Algometer that produces clamping loads (quasi-static contacts)

Subjects hold a three-setting switch during a load test. They were instructed to push the switch to its second setting throughout the test to maintain the force transmission between the hand crank and the rod. Subjects were additionally instructed to push the switch to its third setting the moment the clamping force caused slight pain at the loaded body location. The third setting stops the transmission of force, at which point the rod immediately recoils.

3.1.2 Pendulum for testing transient contacts

The principle of the pendulum (see Figure 4) used to produce impacts resemble a four-bar linkage. Two parallel bars that each measure 0.8 m in length connect the freely hanging pendulum body to the frame, which is connected to a horizontal and a vertical linear guide. Two motors drive the linear guides used to adjust the pendulum body's height and position relative to the subject's body. The guides' motion range in conjunction with platforms and chairs used in the tests enabled us to reach every body location in Figure 2 on subjects ranging from 1.65 to 2.10 m in height.

The moving pendulum body converts its potential energy into kinetic energy upon reaching its deepest point after having been released from a certain height. The moment the pendulum body

strikes a subject, it transfers its kinetic energy to the body location, which transfers part of that energy back to the pendulum body once the maximum force has been reached. A locking lever with thirty equidistant notches, which is mounted on the support frame, deflects the pendulum to a specific height. The thirty notches correspond to thirty different deflections and heights. One of the parallel bars is connected to a rotary potentiometer that records the pendulum angle over time. If necessary, a spring-loaded splint can be added to subdivide the distance between two notches into five segments. The maximum attainable impact velocity is 1.25 m/s. The locking lever and the spring-loaded splint are used to change the impact velocity in increments of approximately 0.01 m/s to approach the subject's pain threshold gradually in a series of consecutive tests.

The pendulum body has an interface that accommodates the attachment of additional weights at its COG (center of gravity) to increase the pendulum's net weight from 1.9 kg to as much as 20 kg. Differently shaped impactors can be attached to a second interface on the face of the pendulum body (see Section 3.1.3). This interface is part of the load cell that records the contact force during a subject test over time.

Unlike the algometer, the pendulum does not have a switch that enables subjects to indicate the onset of pain. Subjects were instructed to say "stop" whenever an impact caused a sensation of slight pain in the body location being tested. As with the algometer, we used straps and vacuum cushions to secure subjects' body parts in a rigid socket.

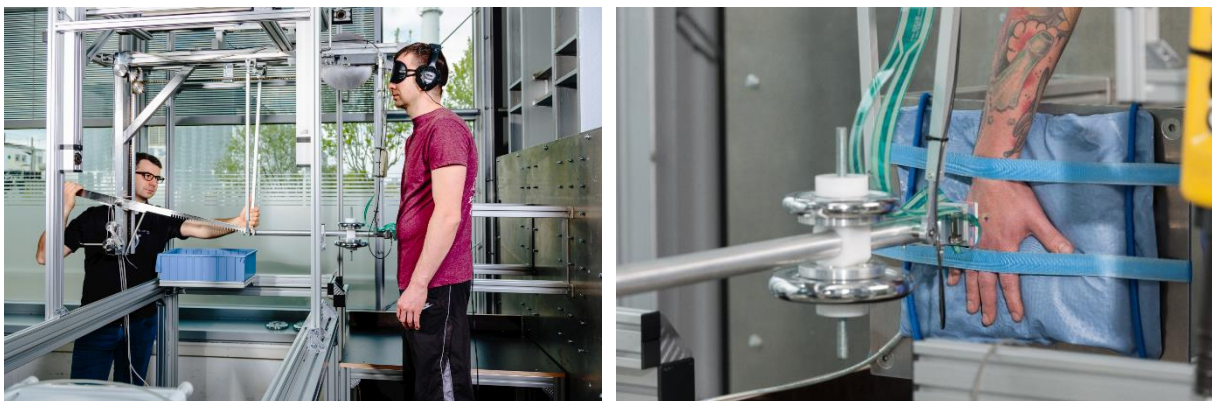


Figure 4. Pendulum that produces impact loads (transient contact)

3.1.3 Contact bodies

We used two different contact bodies, semi-sharp and blunt, to determine pain thresholds (see Figure 5). The semi-sharp contact body F-Q10 is made of aluminum, has a rectangular cross-section and a rounded edge with a 2 mm radius. A piezoelectric pressure foil (see Section Figure 5) was attached to the contact body's face (the gray mesh in Figure 5) to measure the pressure distribution on the surface on F-Q10. The blunt contact body F-Z30 has a much larger contact area than F-Q10 and is made of a compliant foam that distributes the contact force uniformly over the contact area to prevent any incidence of regions with distinct peak pressures.

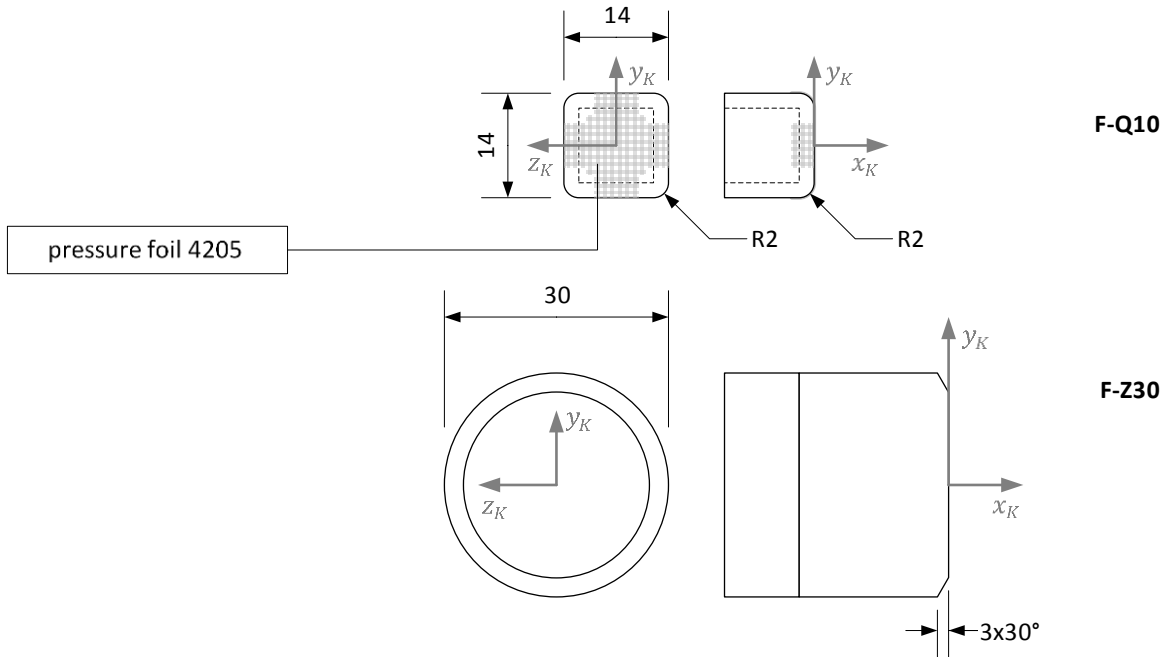


Figure 5. Contact bodies used

3.1.4 Additional provisions

Subjects wore sleep masks and headphones playing nature sounds during the tests. We took both actions to isolate subjects from their surroundings and to preserve the element of surprise. The latter has particularly proven necessary since it also prevents subjects from instinctively tensing their muscles right before being subjected to a clamping or impact load.

3.2 Instrumentation and Equipment

Different sensors are integrated in the algometer and the pendulum. The sensors we used in both systems, the signals they recorded, and the preprocessing methods are examined below.

3.2.1 Algometer

Table 4 presents the sensors we installed on the algometer. We used a piezoelectric load cell to record the contact force $F_C(t) \in \mathbb{R}$ acting along the rod that pushes the attached contact body against the subject's body. The load cell was connected to an amplifier that converted the charge transfer from the load cell into voltage. An inductive encoder placed inside the push mechanism recorded the contact body's displacement $x_C(t) \in \mathbb{R}$. A high-precision resistor converted the sensor's output current signal into voltage. The converted signals from the load cell and the position sensor were fed into a Meilhaus ME-4660i PCIE A/D converter, which sampled the signal with a resolution of 16 bit and a frequency f_S of 100 Hz.

We used a TekScan I-Scan system to measure pressure in the tests with the semi-sharp contact body F-Q10. Since the system can only be used with TekScan software, we were unable to integrate it in our measurement chain to record all signals synchronously at the same sampling rate. What is more, the TekScan system samples pressure with a significantly lower resolution of 8 bits. Since the TekScan system has a trigger signal that indicates when measurements are being taken,

we fed this signal into the A/D converter and used it to synchronize the pressure signal with the other signals.

The pain switch state (see Section 3.1.1) was remapped to a binary switch signal. The switch is “on” as soon as the subject moves it to the second setting. The other settings are concomitant with “off”.

Table 4. Sensors integrated in the algometer

Sensor	Signal	Sampling (Hz)	Range	Type
Load cell (1D)	$F_M(t) \in \mathbb{R}$	200	± 500 N	Kistler, 9311B
Encoder	$z_A(t) \in \mathbb{R}$	200	150 mm	Micro-Epsilon, VIP150
Pressure foil	$[\Psi]_C(t) \in \mathbb{R}^{M \times N}$	200	1.2 kN/cm ²	TekScan, 5120
Pain switch	$P(t) \in \mathbb{R}$	200	10 V	Industrial panic switch

3.2.2 Pendulum

Table 5 presents the sensors we installed on the pendulum. We used a piezoelectric load cell to record the contact force $\mathbf{f}_M(t)$ acting on the contact body in all three spatial directions. The load cell was connected to an amplifier that converted the charge transfer from the load cell into a voltage transmitted to the A/D converter. The position sensor was attached to one of the rear bars and recorded the pendulum angle $\varphi_P(t)$. It was a high-precision potentiometer with a slider that rotated over a circular resistor. The voltage over the slider $u_\varphi(t)$ and the supply voltage U_0 over the resistor were both fed directly into the AD converter. We used the same A/D converter used for the algometer but with a sampling frequency f_s of 10kHz.

Table 5. Sensors integrated into the pendulum

Sensor	Signal	Sampling (Hz)	Range	Type
Load cell (3D)	$\mathbf{f}_M(t) \in \mathbb{R}^{3 \times 1}$	10	± 1 kN	Kistler, 9327C
Potentiometer	$\varphi_P(t) \in \mathbb{R}$	10	$\pm 45^\circ$	Novotechnik, P4500
Pressure foil	$[\Psi]_C(t) \in \mathbb{R}^{M \times N}$	2,04	1.2 kN/cm ²	TekScan, 5120

We also used the TekScan I-Scan system to measure pressure and its trigger output to synchronize the pressure signal’s time axis with the signals’ time axes. Since the TekScan system’s maximum sampling rate is 2.04 kHz, the increments of the pressure signal’s time axis differ from the other signals’ common time axis.

4 Test Procedure

4.1.1 Acquisition of subjects

Once the study design had been finalized and ethical approval had been received, we began to seek volunteers interested in participating in our studies. We used different types of media such as advertisements in local newspapers and on bulletin boards to reach out to the public. This phase was followed by an informational meeting to which we invited all interested individuals who responded to our advertisement. At the meeting, a research scientist from the Fraunhofer IFF and a physician from Otto von Guericke University explained all the details of the study to the attendees. Then they passed out an information sheet summarizing the content of the meeting to all interested attendees. Candidates were given the opportunity to sign up as potential subjects for the study within one week after the meeting.

4.1.2 Selection of subjects

The first step in the selection procedure was to reject all the individuals beyond the employable age in Germany. Then the male and female candidates were divided into two separate groups. We did this to ensure that the selected group of subjects had an equal share of males and females. Afterward, the necessary number of subjects were randomly selected from each of the two groups.

4.1.3 Clinical assessment of the subjects' health

The candidates selected had to have their health assessed before they could finally participate in the study. The physicians only accepted subjects without any preexisting conditions that might cause complications or potentially compromise or bias the results. Apart from conducting clinical assessments, the physicians also determined each subject's dominant body location and ensured that we assigned each of them the right gender. None of the subjects assessed were transgender or non-binary.

4.1.4 Preparation of each session

Before their first session, subjects had to sign a consent form, agreeing to participate in the study and accepting the test conditions. Subjects could decline to sign the consent form without having to provide any reason. Once a subject had signed the consent form, the test supervisor started preparing the load tests. First, the test supervisor inquired after the subject's well-being. In the event that the subject was not feeling well, the test supervisor rescheduled the session for another day. Otherwise, the test supervisor marked the body locations specified by the work-plan for that particular session with a skin-safe marker.

4.1.5 Load test

A single load test denotes the point in a session when we applied clamping or impact loads to the subjects' body parts specified by the work plan for that particular session. The test procedure depends on the load type and the testing system used. The first steps for both systems were nevertheless identical.

Before starting the test, the test supervisor has to secure the body part of the point where the load must be applied. This is done with a variety of means that keep body parts from shifting or

slipping when the load is applied (see Figure 6). We secured body parts in a way that ensured that subjects could stand upright neutrally and relaxed without tensing their muscles unduly. Only a few body locations, e.g. on the head or chest, required subjects to sit or lean forward.

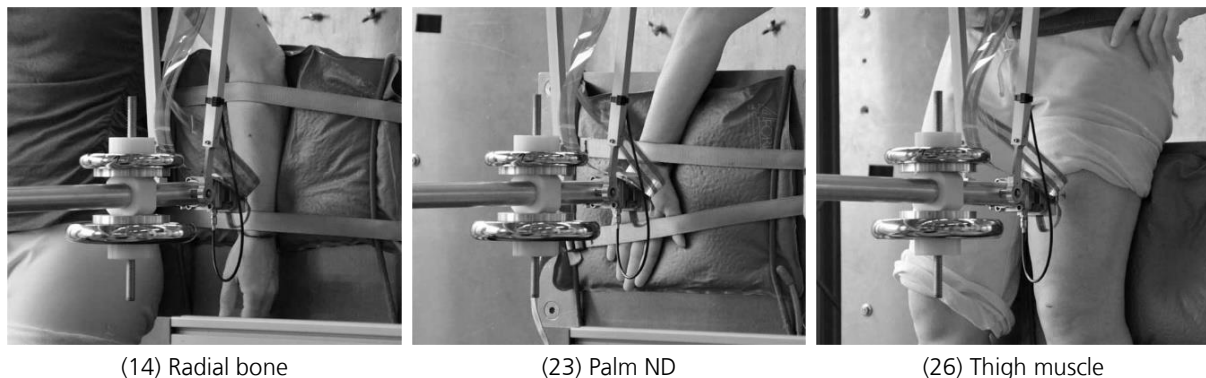


Figure 6. Securing of body parts

Procedure with the algometer

Before preparing the subject for the session, the test supervisor configured the algometer following the session's work plan. As indicated by the work plan for all studies (see Table 1), the algometer's configuration was solely dependent on the contact body. After placing the subject in the algometer and securing their body parts, the test supervisor aimed the contact body attached to the rod precisely at the marked body location so that the clamping force acted perpendicularly to the skin on the body location. Then a sleep mask and headphones playing nature sounds were put on the subject.

Once the subject moved the pain switch to the second setting, the test supervisor began to turn the crank, at which point the rod moved the contact body toward the subject's body. The subject moved the switch to the third setting the moment the continuously increasing clamping force caused the onset of pain and the rod recoiled immediately. Every single test on a single body location was repeated several times (see work plan in Table 1). The final repetition concluded the testing of a particular body location.

Procedure with the pendulum

Before preparing the subject for the session, the test supervisor configured the impact following the session's work plan. As indicated by the work plan for all studies (see Table 1), the pendulum's configuration ensued from the specific combination of mass and contact body. Once the subject had been secured, the test supervisor aimed the free-hanging pendulum body at the marked location on the body part so that the contact body would hit it approximately perpendicularly to the body surface. Then a sleep mask and headphones playing nature sounds were put on the subject.

Afterward, the test supervisor deflected the pendulum body to the starting height and hooked it into the locking lever. Next, the test supervisor started the instruments and released the pendulum by pulling the locking lever up, at which point the pendulum began to move and subsequently hit the subject. Once the pendulum recoiled, the test supervisor caught it at its rear bars and hooked

it at the subsequent height with the locking lever. The instrument controller automatically stopped the signal recording two seconds after the pendulum lost contact with the subject. Then it stored the data in a database.

The test supervisor repeated the procedure with increasing impact velocity until the subject indicated that the most recent of the consecutive impacts caused a slight sensation of pain at the targeted body location. As the impact velocity increased, the test supervisor also increased the energy of the impact. Findings from other research studies do not furnish any clear evidence that sequentially applied brief impacts do not influence the pain threshold significantly.

To finish the test in a minimum of time, we decided to use the highest pendulum mass (~16.2 kg) to perform the first test and to reduce it to the lower mass (~5.8 kg) in the next session scheduled at least three days later. This enabled us to continue with the impact velocity that produced a sensation of pain in the preceding session safely in the next session since the lower mass reduced the impact energy and thus the contact forces significantly.

4.1.6 Follow-up actions

The test supervisor recorded the testing system configuration in the subject's file after every single test. Afterward, the test supervisor released the subject's body part and asked after their well-being to ensure that they were up to testing the next body part. A brief visual examination of the body part tested ensured that there were no visible changes that might indicate a slight injury (e.g. swelling or even slight hemorrhaging).

4.2 Measurement Data Processing

4.2.1 Noise suppression and offset compensation

The recorded signal consisted of various noise components, which had to be suppressed to interpret the data properly. The noise components in the voltage signal entering the A/D converter appeared as a high-frequency noise that was reduced with a low-pass filter. We used a phase-zero and fourth-order Butterworth low-pass filter compliant with SAE J211-1. The automotive sector uses such filters for crash tests. The SAE standard specifies so-called CFC (channel frequency class) filter classes, the identification numbers of which correspond to the filters' cut-off frequencies and structures. An analysis of the signals recorded by the algometer and pendulum instruments revealed that the CFC classes presented in Table 6 suppressed noise sufficiently.

Table 6. Used CFC filter classes for high-frequency noise suppression

System	Signal	CFC class
Algometer	Contact force	1
	Position	1
	Pressure	1
Pendulum	Contact force	100
	Position (angle)	20
	Pressure	100

In addition to suppressing noise, we also compensated the offset in the force signal to correct its zero-point. The charge amplifier added this constant voltage bias so that zero force at the contact body did not correspond to zero voltage. After compensation, the force right before initial contact was precisely zero.

4.2.2 Pressure signal post-processing

We used TekScan's I-Scan system to record the distribution of the force on the face of the contact body F-Q10. A distinctive characteristic of the system's sensors is that image noise interferes with the pressure signals converted and stored as images over time. TekScan recommends applying a Gaussian blur filter to reduce such noise. The gray mesh on F-Q10 in Figure 5 illustrates another issue: Since the TekScan pressure foil 5120 used did not cover the entire face of F-Q10, we decided to apply an interpolation method to fill the blind spots with estimated pressure values. Another problem we encountered was the synchronization of the TekScan system's data with the other instruments' signals since the TekScan system uses a separate AD converter.

Image noise suppression

TekScan supplies a built-in Gaussian filter to suppress image noise but only for images recorded by a flat sensor foil. Since we needed to bend the sensor foil at the edges to cover F-Q10, we had to develop our own spatial Gaussian filter. We decided to use a Gaussian filter with a constant variance of $\sigma^2 = \sqrt{2/\pi}$ and the following position-dependent pulse response

$$h(x, y) = \frac{1}{2\pi\sigma^2} \exp\left\{-\frac{x^2 + y^2}{2\sigma^2}\right\} .$$

Each pixel in a pressure image corresponds to the position of a tiny sensor cell (sensel) covering a finite area on the surface of F-Q10. Bending the foils only necessitates extracting those values from every single pressure image visible in the analyzed projection of the bent sensor (overhead view or one of the four lateral views), which correspond with the sensels. Extraction only has to factor in the force component the sensel can record in the analyzed projection. The normal vectors of the finite areas covered by the sensels yield the correct component. Extraction must also factor in each sensel's position in the analyzed projection plane (see Figure 7).

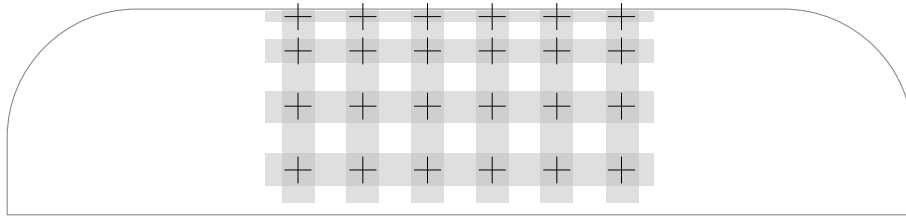


Figure 7. Position of the sensor cells within one of five projections (here: one of four side views)

Once the segment of the analyzed pressure image belonging to the projection has been extracted, we can calculate a filter kernel \mathbf{H}_{ij} for each pixel in the projection. The filter kernel contains discrete values of the Gaussian function $h(x, y)$

$$\mathbf{H}_{ij} = \begin{bmatrix} h(\Delta x_{i-1}, \Delta y_{j-1}) & h(\Delta x_{i-1}, 0) & h(\Delta x_{i-1}, \Delta y_{j+1}) \\ h(0, \Delta y_{j-1}) & h(0, 0) & h(0, \Delta y_{j+1}) \\ h(\Delta x_{i+1}, \Delta y_{j-1}) & h(\Delta x_{i+1}, 0) & h(\Delta x_{i+1}, \Delta y_{j+1}) \end{bmatrix},$$

where Δx and Δy are the geometric distances from pixel p_{ij} to its adjacent neighbors. Then matrix \mathbf{H}_{ij} must be multiplied element-wise into the image matrix formed by p_{ij} and its neighbors. Afterward, the sum of the multiplied pixels yields the filtered pixel \tilde{p}_{ij}

$$\tilde{p}_{ij} = \sum_{m=-1}^1 \sum_{n=-1}^1 h(\Delta x_{i+n}, \Delta y_{j+m}) p_{(i+n)(j+m)} .$$

We applied this filtering procedure to all images for each pressure measurement over time. Figure 8 presents an example of filtering results.

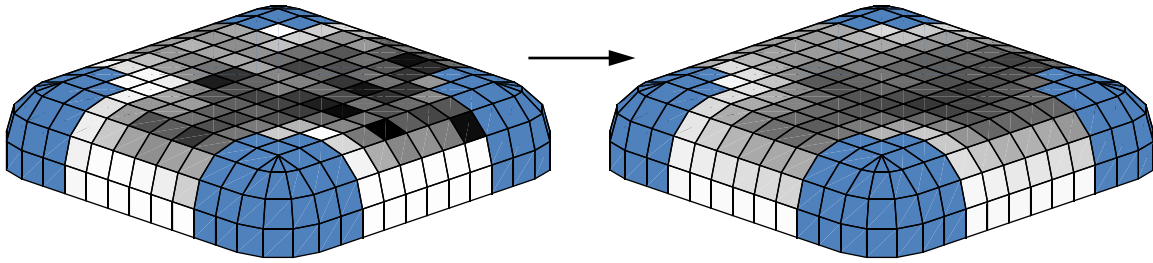


Figure 8. Pressure image before (left) and after image denoising by a spatial Gaussian blur filter (right)

Estimation of pressure values in the contact area's blind spots

We used an interpolation method to estimate the pressure values unavailable for the spots not covered by the pressure foil on F-Q10. Figure 9 visualizes our method's main principle. First, all values lying on the same contour as the contact body are extracted from the pressure image. Plotting these values as a function of their position on the contour yields a broken curve with apparent gaps (see the diagram in Figure 9). Our method closed these gaps with linear interpolation. Repeating the procedure for all contours and open gaps ultimately produces a contact area entirely covered with estimated pressure values.

Pressure signal synchronization with other signals

In some tests, the TekScan system's constraints required us to sample the pressure signal at a significantly lower rate than the other signals. The pressure values were therefore not synchronous with those of the force over time, thus making it very difficult to use the force values for post-test calibration of the pressure values because the pressure integrated over the contact area must correspond to the contact force.

The TekScan system has a trigger output that indicates when the system is recording, though. We fed this signal into the AD converter and used it later to synchronize the time axis of the pressure with the time axis of the other signals, including force. Then we used an interpolation algorithm to increase the resolution of the pressure signal artificially to the resolution of the other signals.

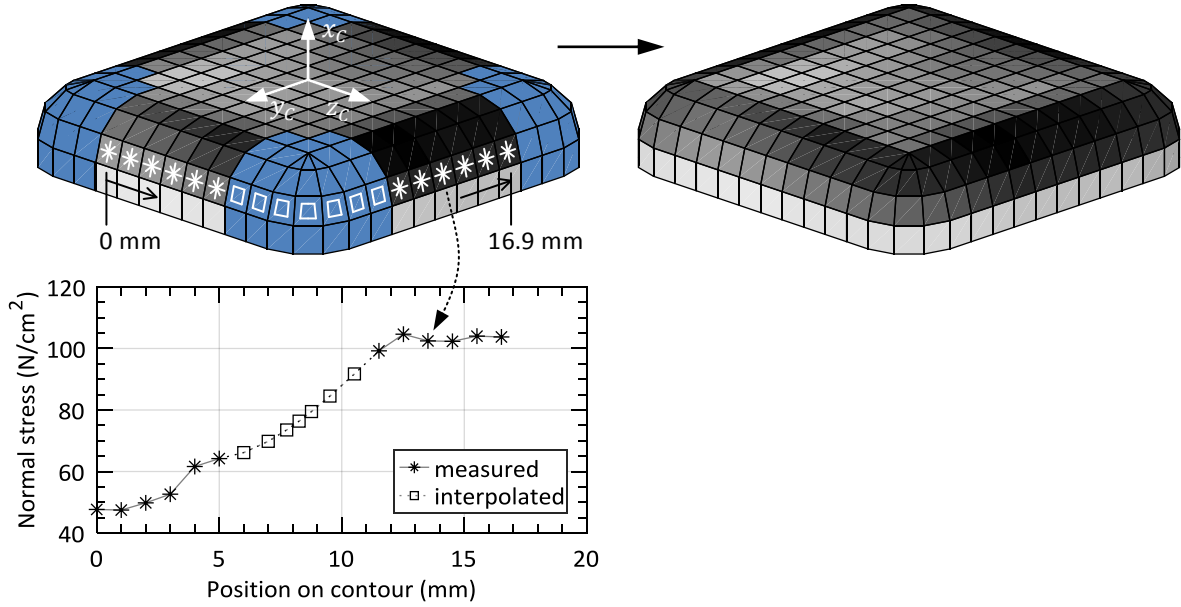


Figure 9. Interpolation applied to estimate the pressure values in the blind spot of probe F-Q10

4.2.3 Post-processing of the signals recorded at the pendulum

The dynamics and kinematics of the pendulum required a special conversion of the recorded signals to process and analyze them further. The additional post-processing steps we applied to the data acquired with the pendulum are explained briefly below.

Compensation of inertial effects

Since the entire pendulum mass (body mass m_B including contact body mass m_I) acts on the contact point, while only the pendulum body mass m_B acts on the sensor, the load cell's position between the pendulum body and the contact body reduced the force transmitted to the load cell so that the measured force $\mathbf{f}_M(t) \in \mathbb{R}^{3 \times 1}$ did not correspond to the actual contact force $\mathbf{f}_C(t) \in \mathbb{R}^{3 \times 1}$ (Nahum et al. 1972; Stalnaker und Melvin 1976). This effect can be compensated by scaling the measured force \mathbf{f}_M up to the desired contact force \mathbf{f}_C with

$$\mathbf{f}_C = V_f \mathbf{f}_M \quad .$$

The required factor is

$$V_f = 1 + \frac{m_I}{m_B}$$

where m_I is the mass of the contact body and m_B the mass of the pendulum body.

Determination of impact velocity

Impact velocity $\dot{\mathbf{x}}_{C0}$ is produced by the pendulum radius r_p and the pendulum's angular velocity ω_{p0} at time t_0 representing the moment of initial contact

$$\dot{\mathbf{x}}_{C0} = r_p \omega_{p0} [\cos \varphi_{p0} \quad \sin \varphi_{p0} \quad 0]^T \quad .$$

The angular velocity ω_{P0} is the slope of the tangent of the position signal $\varphi_P(t)$ at time t_0 with $\varphi_{P0} = \varphi_P(t_0)$ and ultimately yields the desired pendulum velocity. The magnitude of the impact velocity v_{P0} is

$$v_{P0} = \|\dot{\mathbf{x}}_{K0}\| \quad .$$

5 Results

5.1 Subjects

The number of subjects varied from study to study. Table 7 presents the different groups arranged by gender. The larger number of males in groups #1, #2, and #3 goes back to our wish to have at least 30% of the subjects be blue-collar workers paired with our inability to recruit enough female blue-collar workers to keep the gender distribution equal. The data analyzed did not reveal any significant difference between the pain thresholds of subjects working in industry and those who do not, though. This finding prompted us to discard our requirement for the makeup of the groups of subjects, thus distributing males and females equally in groups #4 and #5.

Table 7. Body parameters of the subjects that participated in our studies

Group	Gender	Number	Age (y)	Height (m)	Weight (kg)	BMI (kg/m ²)
#1	Female	13	41.3±14.5	1.67±0.08	65.2±9.0	23.2±2.2
	Male	28	40.2±14.0	1.81±0.07	86.3±14.7	26.5±4.7
	Mixed	41	40.6±14.0	1.77±0.10	79.6±16.4	25.4±4.3
#2	Female	6	43.8±14.5	1.72±0.08	67.5±11.7	22.8±2.9
	Male	14	41.0±15.0	1.79±0.07	83.2±13.8	25.9±4.9
	Mixed	20	41.9±14.5	1.77±0.08	78.5±14.9	25.0±4.6
#3	Female	10	39.7±13.6	1.69±0.07	80.3±23.6	28.0±7.4
	Male	10	40.7±14.5	1.79±0.04	80.7±7.0	25.3±2.3
	Mixed	20	40.2±13.7	1.74±0.08	80.5±17.0	26.7±5.5
#2 + #3	Female	16	41.3±13.6	1.70±0.07	75.5±20.5	26.0±6.5
	Male	24	40.9±14.5	1.79±0.06	82.2±11.3	25.7±4.0
	Mixed	20	41.0±13.9	1.76±0.08	79.5±15.8	25.8±5.1
#4	Female	10	38.7±13.8	1.66±0.06	63.3±8.7	22.9±2.8
	Male	10	39.2±14.8	1.81±0.07	84.3±18.5	25.6±4.6
	Mixed	20	39.0±14.0	1.74±0.10	73.8±17.7	24.3±4.0
#5	Female	5	36.6±14.5	1.67±0.06	58.0±2.7	20.8±0.9
	Male	6	36.0±13.8	1.80±0.04	78.3±4.8	24.2±1.2
	Mixed	11	36.3±13.4	1.74±0.08	69.1±11.3	22.7±2.0

Table 8 breaks down the test data from the groups of subjects, which we used to ascertain pain thresholds for both load and contact types. The plan shows that we only performed impact tests on locations on the dominant side. This was prompted by our finding that the pain thresholds of the dominant hand are significantly higher than those of the non-dominant hand and the failure of standard risk assessment to distinguish between dominant and non-dominant sides.

Table 8. Assignment of the subject groups to the tested body locations

Body part	Body location	Quasi-static		Transient	
		Semi-sharp*	Blunt	Semi-sharp	Blunt
Head and neck	(1) Forehead	#5	#4	#4	#4
	(2) Temple	#5	#4	#4	#4
	(3) Masticatory muscle	#5	#4	#4	#4
	(4) Neck muscle	-	-	-	-
	(5) 7th cervical vertebra	#5	#4	#4	#4
Trunk	(6) Shoulder joint	#5	#1	#2 + #3	#2 + #3
	(7) 5th lumbar vertebra	#5	#1	#2 + #3	#2 + #3
	(8) Sternum	#5	#1	#4	#4
	(9) Pectoral muscle	#5	#1	#4	#4
	(10) Abdominal muscle	#5	#1	#4	#4
	(11) Pelvic bone	#5	#1	#2 + #3	#2 + #3
Upper extremities	(12) Deltoid muscle	#5	#1	#2 + #3	#2 + #3
	(13) Humerus	#5	#1	#2 + #3	#2 + #3
	(14) Radial bone	#5	#1	#2 + #3	#2 + #3
	(15) Forearm muscle	#5	#1	#2 + #3	#2 + #3
	(16) Arm nerve	#5	#1	#2 + #3	#2 + #3
Hand and fingers	(17) Forefinger pad D	#5	#1	#2	#2
	(18) Forefinger pad ND	#5	#1	#2 + #3	#2 + #3
	(19) Forefinger end joint D	#5	#1	#2	#2
	(20) Forefinger end joint ND	#5	#1	#2 + #3	#2 + #3
	(21) Thenar eminence	#5	#1	#2 + #3	#2 + #3
	(22) Palm D	#5	#1	#2	#2
	(23) Palm ND	#5	#1	#2 + #3	#2 + #3
	(24) Back of the hand D	#5	#1	#2	#2
	(25) Back of the hand ND	#5	#1	#2 + #3	#2 + #3
	(26) Thigh muscle	#5	#1	#2 + #3	#2 + #3
Lower extremities	(27) Kneecap	#5	#1	#2 + #3	#2 + #3
	(28) Middle of shin	#5	#1	#2 + #3	#2 + #3
	(29) Calf muscle	#5	#1	#2 + #3	#2 + #3

*) control group

5.2 Usable data

We obtained approximately 29,000 individual results from the tests in all the studies. Results are unavailable for some subjects for a variety of reasons. Table 9 presents reasons for missing data, most of which are the physicians' clinical assessments.

Table 9. Missing data

Subject	Body location	Contact body	Impact mass	Reason
1002	(13) Humerus (15) Forearm muscle	F-Z30	16.2 kg; 5.8 kg	Recording error
1009	(6) Shoulder joint (12) Deltoid Muscle (13) Humerus	F-Q10	16.2 kg; 5.8 kg	No medical clearance
1012	all	all	5.8 kg	Subject left study
1014	(25) Back of the hand ND	F-Q10; F-Z30	5.8 kg; 16.2 kg	No medical clearance
1019	(27) Kneecap	all	all	No medical clearance
2004	(7) 5th lumbar vertebra	all	all	No medical clearance
4002	(7) 5th lumbar vertebra	F-Q10	-	No medical clearance
4003	(7) 5th lumbar vertebra	F-Q10	-	No medical clearance

5.3 Output Variables

Output variables reference the effect of a load on the human body with usable mechanical limits. Following FBHM 080 and ISO/TS 15066, we used the output variables of *maximum contact force* and *maximum peak pressure* (maximum normal stress) to define the desired pain thresholds.

Maximum contact force

Maximum contact force \hat{F}_C is the strongest force acting on the body location when an external impact or clamping load is applied

$$\hat{F}_C = \max_t F_C(t) \quad 0 \leq t \leq \tau_C$$

where τ_C is the period of contact

$$\tau_C := \{\Delta t \mid F_C(t_0 < t < (t_0 + \Delta t)) > 0\} \quad .$$

In the event the contact force is a vector over time, the Euclidian vector norm yields the magnitude $F_C(t)$

$$F_C(t) = \|\mathbf{f}_C(t)\| \quad .$$

Maximum pressure

Maximum pressure $\hat{\psi}_C$ is the strongest pressure in the contact area produced by the load on the surface of the contact body $\partial\mathbf{x}$

$$\hat{\psi}_C = \max_{t;\mathbf{x}} \psi_C(t, \mathbf{x}) \quad 0 \leq t \leq \tau_C \quad \mathbf{x} \in \partial\mathbf{x} \quad .$$

Maximum deformation

Maximum deformation \hat{x}_D is the greatest deformation of soft tissue at the loaded body location

$$\hat{x}_D = \max_t x_I(t) \quad 0 \leq t \leq \tau_C$$

where $x_I(t)$ is the position of the contact body, which is zero at the moment of initial contact with the subject $x_I(0) = 0$.

5.4 Statistics

5.4.1 Data censoring

The distinctive impact test data require conversion before they can be analyzed them with standard statistical methods. As mentioned in Section 4.1.5, we approached the subjects' pain threshold by gradually increasing the impact energy. This procedure renders the real threshold z unknown. Since the only information we have is that z lies within the interval spanning the values from the last two tests, we need to find a way to convert the interval to estimate all subjects' individual pain thresholds in order to identify a threshold for the entire population.

We used midpoint-imputation, which estimates z based on the mean of its intervals (Sun 2006). The left boundary L always has the value of the output variable measured in the next-to-last test, which does not cause any pain, while the right boundary R has the value from the final test, which causes pain. In the unlikely but possible event that the very first test causes pain, the observation is left-censored, meaning the left boundary is $L = 0$, and the right boundary is the value of the output variable measured. A second exception arises when even the highest potential impact velocity does not cause the subject any pain. Then the observation is right-censored $R \rightarrow \infty$. The combination of all cases yields the following expression to estimate z

$$z = \begin{cases} \frac{1}{2}R & L = 0 \\ L & R \rightarrow \infty \\ \frac{1}{2}(L + R) & \text{else} \end{cases} .$$

Figure 10 presents the censored data from randomly selected samples from tests on body location (27). It shows how the maximum pressure increases as the series of tests progresses. The results from all final two measurements comprise the estimated individual pain threshold, which we will include in the calculation of the threshold for the entire population.

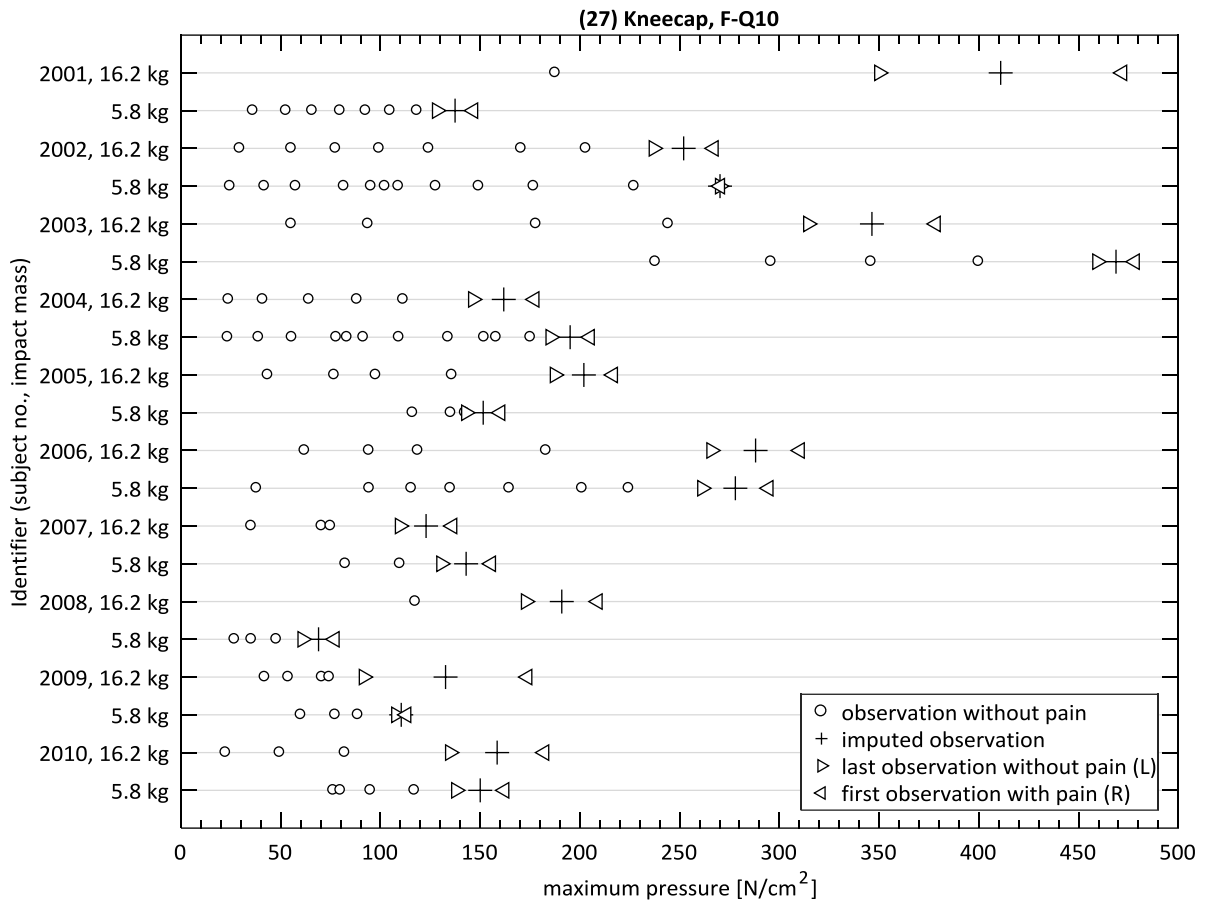


Figure 10. Samples of interval-censored data from impact tests

5.4.2 Descriptive statistics

Descriptive statistics supplies various tabulated measures of tendency and variability to compile an overview of the data. Box plots complement the tables and qualitatively outline the distribution of the empirical data. Table 10 lists the tables and box plots in this report.

Table 10. List of all tables and box plots of tested contact cases

Load type	Contact type	Contact body	Output value	Descriptive statistics	Box plot
Quasi-static	Semi-sharp	F-Q10	Max. pressure	Table 11, page 25	Figure 11, page 26
	Semi-sharp	F-Q10	Max. force	Table 12, page 27	Figure 12, page 28
	Semi-sharp	F-Q10	Max. deformation	Table 13, page 29	Figure 13, page 30
	Blunt	F-Z30	Max. force	Table 14, page 31	Figure 14, page 32
Transient	Semi-sharp	F-Q10	Max. pressure	Table 15, page 33	Figure 15, page 34
	Semi-sharp	F-Q10	Max. force	Table 16, page 35	Figure 16, page 36
	Semi-sharp	F-Q10	Max. deformation	Table 17, page 37	Figure 17, page 38
	Blunt	F-Z30	Max. force	Table 18, page 39	Figure 18, page 40

Table 11. Descriptive statistics of quasi-static and semi-sharp contact (quasi-static pressure limits; **control group**)

Load type	quasi-static (clamping)							
Contact type	semi-sharp (pressure-based limits)							
Body part	Body location	Maximum pressure [N/cm ²]						N
		AVG	STD	MIN	MED	MAX	Q3	
Head and neck	(1) Forehead	75.1	52.6	7.4	63.6	213.9	109.7	35
	(2) Temple	43.7	27.7	10.9	38.4	142.2	57.5	32
	(3) Masticatory muscle	31.4	19.9	8.0	26.2	86.3	31.6	32
	(4) Neck muscle	-	-	-	-	-	-	-
	(5) 7th cervical vertebra	57.4	34.7	11.1	51.3	130.7	73.2	32
Trunk	(6) Shoulder joint	56.9	51.3	11.8	37.6	257.9	57.2	36
	(7) 5th lumbar vertebra	53.1	46.3	5.6	31.7	166.9	65.8	30
	(8) Sternum	44.1	28.9	8.6	32.2	122.1	65.4	36
	(9) Pectoral muscle	43.8	20.2	21.5	35.7	81.4	60.5	18
	(10) Abdominal muscle	33.6	26.5	6.4	25.1	130.9	40.4	38
	(11) Pelvic bone	129.7	135.0	16.5	58.5	618.5	240.2	35
Upper extremities	(12) Deltoid muscle	65.9	51.4	14.4	47.4	200.3	86.3	39
	(13) Humerus	46.3	34.4	9.2	31.5	128.7	55.2	38
	(14) Radial bone	63.4	53.6	5.2	48.8	233.0	76.9	36
	(15) Forearm muscle	59.7	76.6	9.2	35.4	407.3	59.6	39
	(16) Arm nerve	49.7	38.1	9.7	34.8	135.5	70.1	36
Hand and fingers	(17) Forefinger pad D	67.6	41.0	11.4	60.5	157.7	96.3	36
	(18) Forefinger pad ND	61.6	41.5	9.6	53.4	154.7	75.5	39
	(19) Forefinger end joint D	109.1	70.1	23.3	100.2	330.8	141.3	36
	(20) Forefinger end joint ND	118.7	70.7	17.0	107.4	307.5	145.0	31
	(21) Thenar eminence	46.9	25.7	13.5	44.8	115.8	59.3	36
	(22) Palm D	59.2	31.0	10.7	54.8	160.5	74.2	36
	(23) Palm ND	55.5	37.3	18.8	46.4	203.5	67.1	38
	(24) Back of the hand D	151.1	109.7	48.7	123.4	537.9	169.3	36
	(25) Back of the hand ND	146.9	95.5	44.0	134.9	484.2	175.3	38
Lower extremities	(26) Thigh muscle	63.6	44.1	12.6	50.3	188.0	78.1	39
	(27) Kneecap	102.7	77.5	10.9	77.1	276.2	131.5	36
	(28) Middle of shin	121.7	92.6	13.3	91.5	353.1	209.9	37
	(29) Calf muscle	61.7	44.8	9.1	49.6	201.4	79.3	39

AVG = mean; STD = standard deviation; MIN = minimum; MED = median; MAX = maximum; Q3 = third quartile; N = sample size

Figure 11. Empirical distribution of the data from quasi-static and semi-sharp contact (quasi-static pressure limits; **control group**)

Load type	quasi-static (clamping)
Contact type	semi-sharp (pressure-based limits)

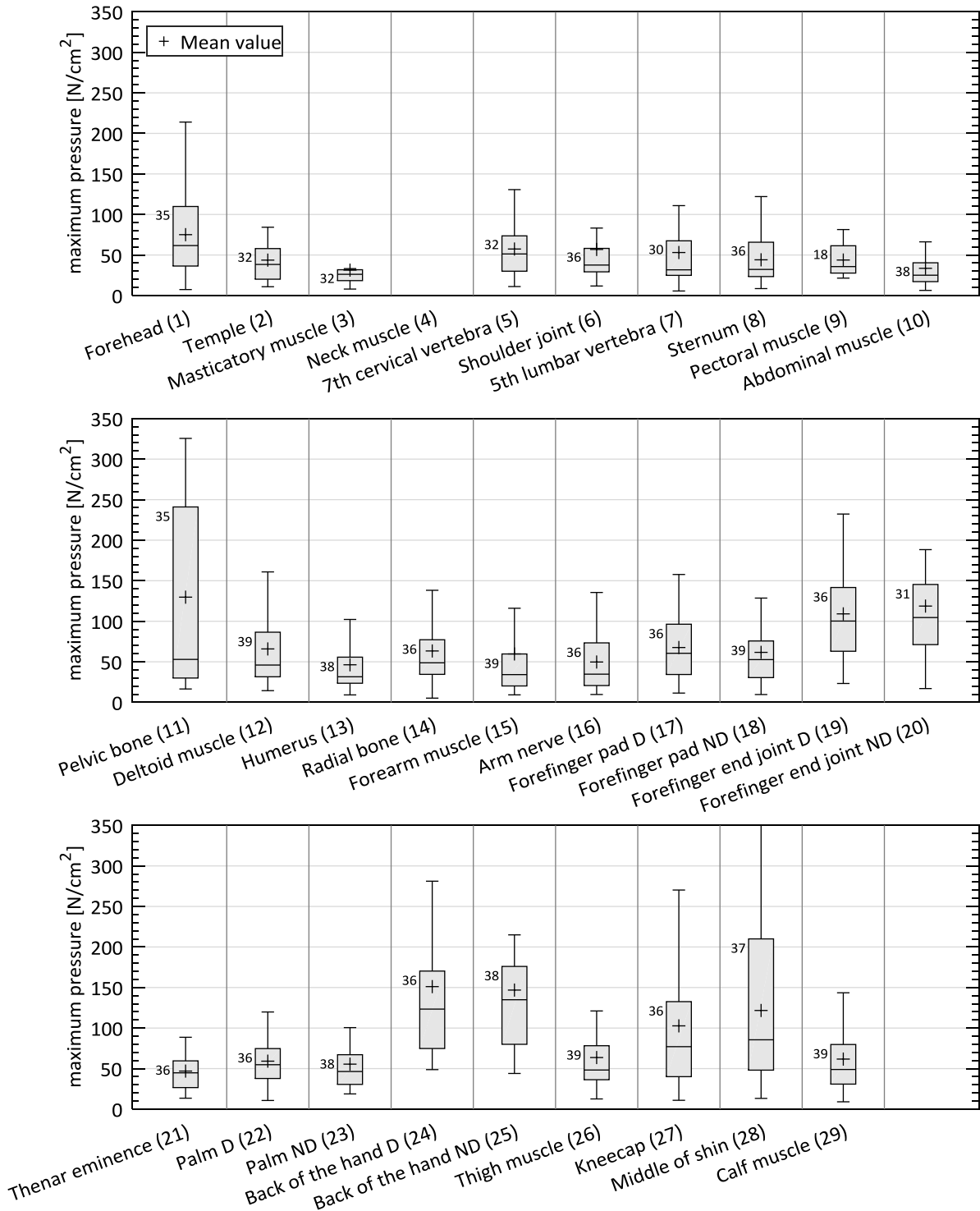


Table 12. Descriptive statistics of quasi-static and semi-sharp contact (maximum contact force; control group)

Load type	quasi-static (clamping)							
Contact type	semi-sharp							
Body part	Body location	Maximum contact force [N]						N
		AVG	STD	MIN	MED	MAX	Q3	
Head and neck	(1) Forehead	46.8	40.8	2	31.7	166.1	74.4	35
	(2) Temple	29.3	23.2	5.3	21.6	114.1	39.3	32
	(3) Masticatory muscle	21.2	15.3	5.1	14.2	63.5	28.4	32
	(4) Neck muscle	-	-	-	-	-	-	-
	(5) 7th cervical vertebra	28.5	23.5	0.5	23.2	84.5	40	31
Trunk	(6) Shoulder joint	37.8	27.8	7.6	27.9	115.1	51.1	36
	(7) 5th lumbar vertebra	47.8	44.6	2.4	30.6	156.1	45.9	30
	(8) Sternum	40.9	40.3	3.4	21.4	155	65.2	36
	(9) Pectoral muscle	36.5	19.4	13	28.7	77.4	53.6	18
	(10) Abdominal muscle	28.4	25.6	4.3	18.5	104.7	33.9	38
	(11) Pelvic bone	53.1	55.1	6.4	32.6	268.4	80	35
Upper extremities	(12) Deltoid muscle	49.1	43.7	8.8	31	178.2	57.3	39
	(13) Humerus	37.5	26.2	3.2	30.5	99.6	51	38
	(14) Radial bone	51.1	48.6	2.4	34.5	212.4	67.7	36
	(15) Forearm muscle	51.7	47.4	6.2	35.1	189.4	64	39
	(16) Arm nerve	38.8	38.6	4.4	20.4	144.2	59.6	36
Hand and fingers	(17) Forefinger pad D	68.2	51.9	6.5	57.4	195.7	89.9	36
	(18) Forefinger pad ND	56.3	45.9	6.3	47.2	190.1	73.6	39
	(19) Forefinger end joint D	46	35.6	9.2	42.6	151.5	57.8	36
	(20) Forefinger end joint ND	49.8	36.5	7.2	42.5	149.5	59.5	31
	(21) Thenar eminence	45.7	35.4	5.5	42.3	130.7	66	36
	(22) Palm D	54.9	36.5	5.1	49.1	145.7	70.1	36
	(23) Palm ND	54.3	43.7	9.2	43.3	200.6	73.6	38
	(24) Back of the hand D	43.6	26.5	4.4	42.6	132.8	58.2	36
	(25) Back of the hand ND	44.5	32.2	13.1	35.8	187.6	56.4	38
Lower extremities	(26) Thigh muscle	66.2	49.1	7.4	52.5	224.9	81.4	39
	(27) Kneecap	81.9	62.7	6.7	62.4	226.6	110	36
	(28) Middle of shin	49.9	30.2	0.4	44.8	112.3	71.6	37
	(29) Calf muscle	57.2	37.4	6.4	50.5	155.4	76	39

AVG = mean; STD = standard deviation; MIN = minimum; MED = median; MAX = maximum; Q3 = third quartile; N = sample size

Figure 12. Empirical distribution of the data from quasi-static and semi-sharp contact (maximum contact force; **control group**)

Load type	quasi-static (clamping)
Contact type	semi-sharp

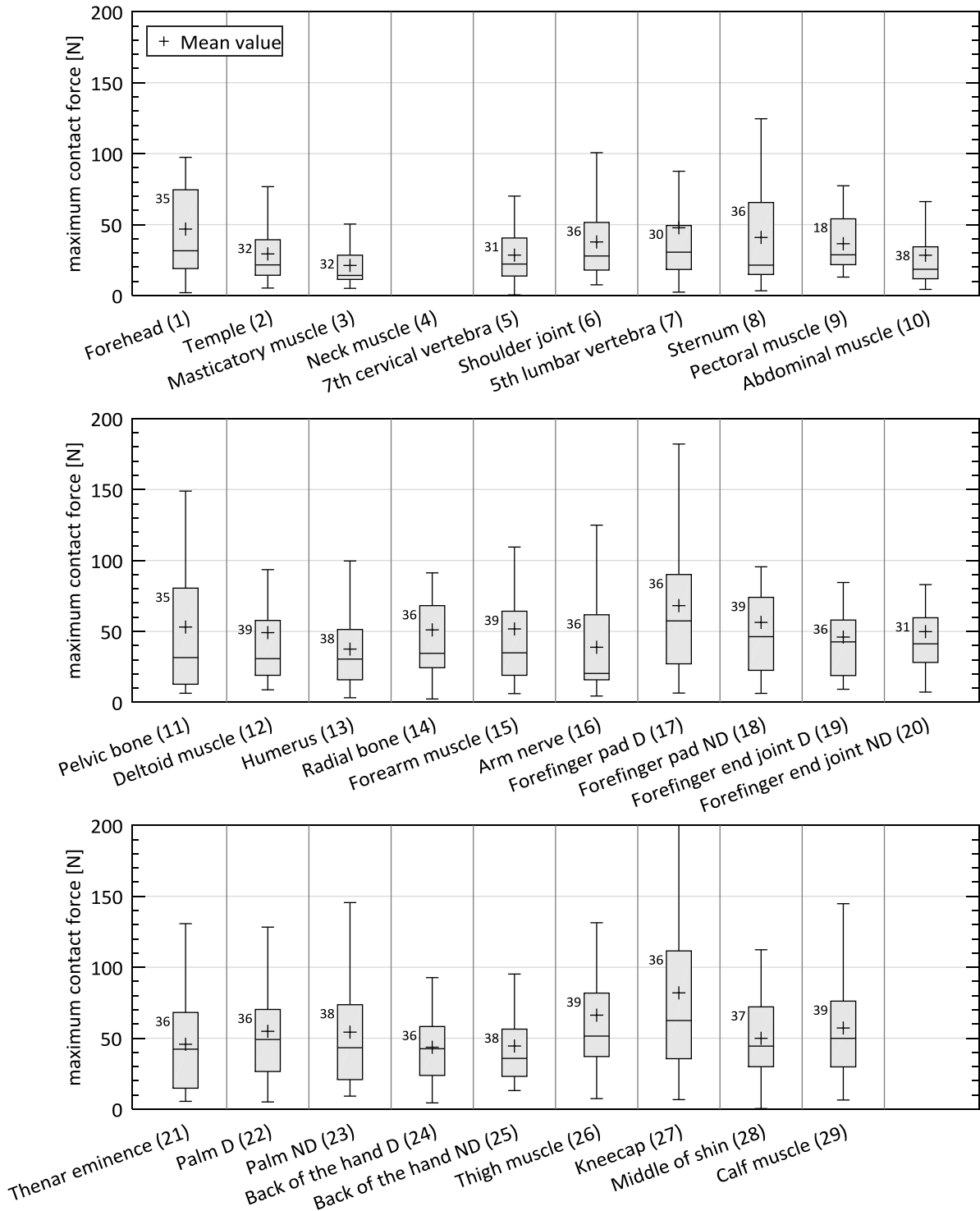


Table 13. Descriptive statistics of quasi-static and semi-sharp contact (maximum deformation; **control group**)

Load type	quasi-static (clamping)							
Contact type	semi-sharp							
Body part	Body location	Maximum deformation [mm]						N
		AVG	STD	MIN	MED	MAX	Q3	
Head and neck	(1) Forehead	2.0	1.5	<0.1	1.7	7.1	2.4	32
	(2) Temple	3.1	1.8	0.6	2.7	8.0	3.9	29
	(3) Masticatory muscle	6.7	4.4	2.0	4.9	20.0	8.2	32
	(4) Neck muscle	-	-	-	-	-	-	-
	(5) 7th cervical vertebra	7.4	5.4	0.3	6.4	24.5	9.1	29
Trunk	(6) Shoulder joint	17.2	10.7	5.0	14.1	50.3	21.4	36
	(7) 5th lumbar vertebra	15.4	7.6	0.7	14.8	30.2	17.9	30
	(8) Sternum	9.2	8.0	0.9	7.0	32.6	12.5	36
	(9) Pectoral muscle	28.0	14.0	12.1	21.8	56.9	34.1	18
	(10) Abdominal muscle	47.8	23.8	11.4	46.1	98.4	61.2	38
	(11) Pelvic bone	11.4	5.7	1.0	11.0	27.2	14.2	35
Upper extremities	(12) Deltoid muscle	33.1	16.0	13.6	29.2	62.7	41.3	39
	(13) Humerus	15.5	4.8	5.0	14.3	25.1	19.7	38
	(14) Radial bone	8.0	3.7	0.5	7.7	17.0	10.3	36
	(15) Forearm muscle	14.0	6.0	4.2	15.2	31.2	17.3	39
	(16) Arm nerve	14.5	6.8	4.5	12.9	29.9	18.4	36
Hand and fingers	(17) Forefinger pad D	6.8	3.0	2.3	6.2	15.2	7.9	36
	(18) Forefinger pad ND	6.4	3.1	1.8	6.1	14.5	8.2	39
	(19) Forefinger end joint D	4.0	2.0	1.1	3.7	10.0	4.9	36
	(20) Forefinger end joint ND	4.2	2.4	0.8	3.8	11.1	5.1	31
	(21) Thenar eminence	12.9	5.0	4.2	14.4	20.6	16.1	36
	(22) Palm D	11.3	3.7	2.9	11.8	17.3	13.8	36
	(23) Palm ND	10.9	4.1	4.3	10.0	20.7	12.8	38
	(24) Back of the hand D	4.0	1.4	1.6	3.8	7.2	5.1	36
	(25) Back of the hand ND	4.3	2.1	1.8	3.7	11.4	5.8	38
Lower extremities	(26) Thigh muscle	35.5	13.3	10.8	38.9	56.3	46.6	39
	(27) Kneecap	6.7	2.9	1.6	6.3	12.6	8.3	36
	(28) Middle of shin	7.6	4.5	0.5	7.3	20.5	9.5	37
	(29) Calf muscle	32.0	9.2	9.3	33.7	48.5	37.9	39

AVG = mean; STD = standard deviation; MIN = minimum; MED = median; MAX = maximum; Q3 = third quartile; N = sample size

Figure 13. Empirical distribution of the data from quasi-static and semi-sharp contact (maximum deformation; **control group**)

Load type	quasi-static (clamping)
Contact type	semi-sharp

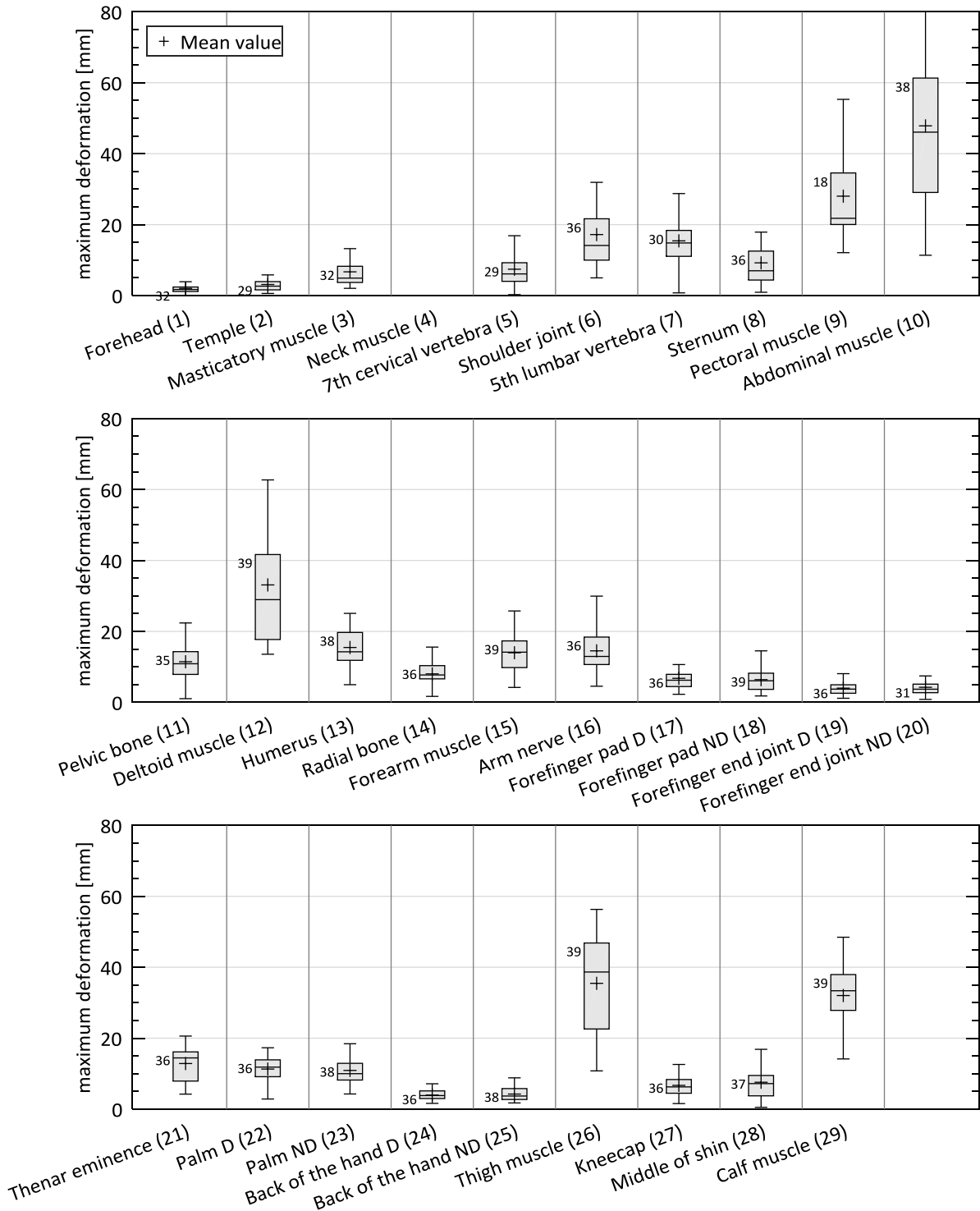


Table 14. Descriptive statistics of quasi-static and blunt contact (quasi-static force limits)

Load type	quasi-static (clamping)							
Contact type	blunt (force-based limits)							
Body part	Body location	Maximum force [N]						N
		AVG	STD	MIN	MED	MAX	Q3	
Head and neck	(1) Forehead	77.2	58.9	2.8	76.1	294.1	103.2	58
	(2) Temple	49.7	45.1	4.2	35.5	219.5	70.0	56
	(3) Masticatory muscle	30.6	23.2	3.9	22.1	86.4	51.1	54
	(4) Neck muscle	-	-	-	-	-	-	-
	(5) 7th cervical vertebra	38.5	32.1	0.6	33.3	146.1	52.5	56
Trunk	(6) Shoulder joint	56.7	25.3	16.3	51.7	167.5	68.5	200
	(7) 5th lumbar vertebra	89.5	63.5	18.7	74.5	322.5	97.2	199
	(8) Sternum	64.9	34.3	9.9	59.0	158.3	90.0	200
	(9) Pectoral muscle	50.0	21.9	9.5	44.7	110.4	63.9	134
	(10) Abdominal muscle	43.2	28.1	5.2	35.5	157.0	62.8	194
	(11) Pelvic bone	77.4	46.2	17.6	68.2	273.4	98.0	197
Upper extremities	(12) Deltoid muscle	84.9	61.5	11.9	61.0	344.6	102.7	197
	(13) Humerus	59.1	30.6	12.3	55.1	189.6	70.8	202
	(14) Radial bone	81.4	42.4	21.0	70.4	256.8	108.3	201
	(15) Forearm muscle	82.6	46.1	19.9	75.5	325.4	104.3	196
	(16) Arm nerve	63.3	30.6	7.2	56.8	165.8	85.9	200
Hand and fingers	(17) Forefinger pad D	137.3	97.4	20.5	114.9	590.3	169.1	189
	(18) Forefinger pad ND	123.2	86.6	9.8	100.3	428.3	159.0	199
	(19) Forefinger end joint D	129.2	70.3	15.7	113.2	346.4	156.6	192
	(20) Forefinger end joint ND	124.4	78.0	7.5	97.0	410.1	165.4	199
	(21) Thenar eminence	100.4	62.7	22.0	87.5	378.4	125.9	197
	(22) Palm D	138.3	89.7	4.2	119.9	511.7	191.8	192
	(23) Palm ND	121.1	83.3	6.4	100.2	524.8	164.6	200
	(24) Back of the hand D	119.9	54.7	31.6	115.8	287.3	147.9	190
	(25) Back of the hand ND	113.1	52.4	20.8	106.7	263.1	143.3	196
Lower extremities	(26) Thigh muscle	119.9	63.5	32.6	106.4	305.6	162.1	193
	(27) Kneecap	128.9	74.5	19.3	102.8	358.0	174.5	191
	(28) Middle of shin	127.7	62.8	50.6	111.2	359.1	146.1	196
	(29) Calf muscle	113.0	62.8	27.8	99.4	337.1	146.6	197

AVG = mean; STD = standard deviation; MIN = minimum; MED = median; MAX = maximum; Q3 = third quartile; N = sample size

Figure 14. Empirical distribution of the data from quasi-static and blunt contact (quasi-static force limits)

Load type	quasi-static (clamping)
Contact type	blunt (force-based limits)

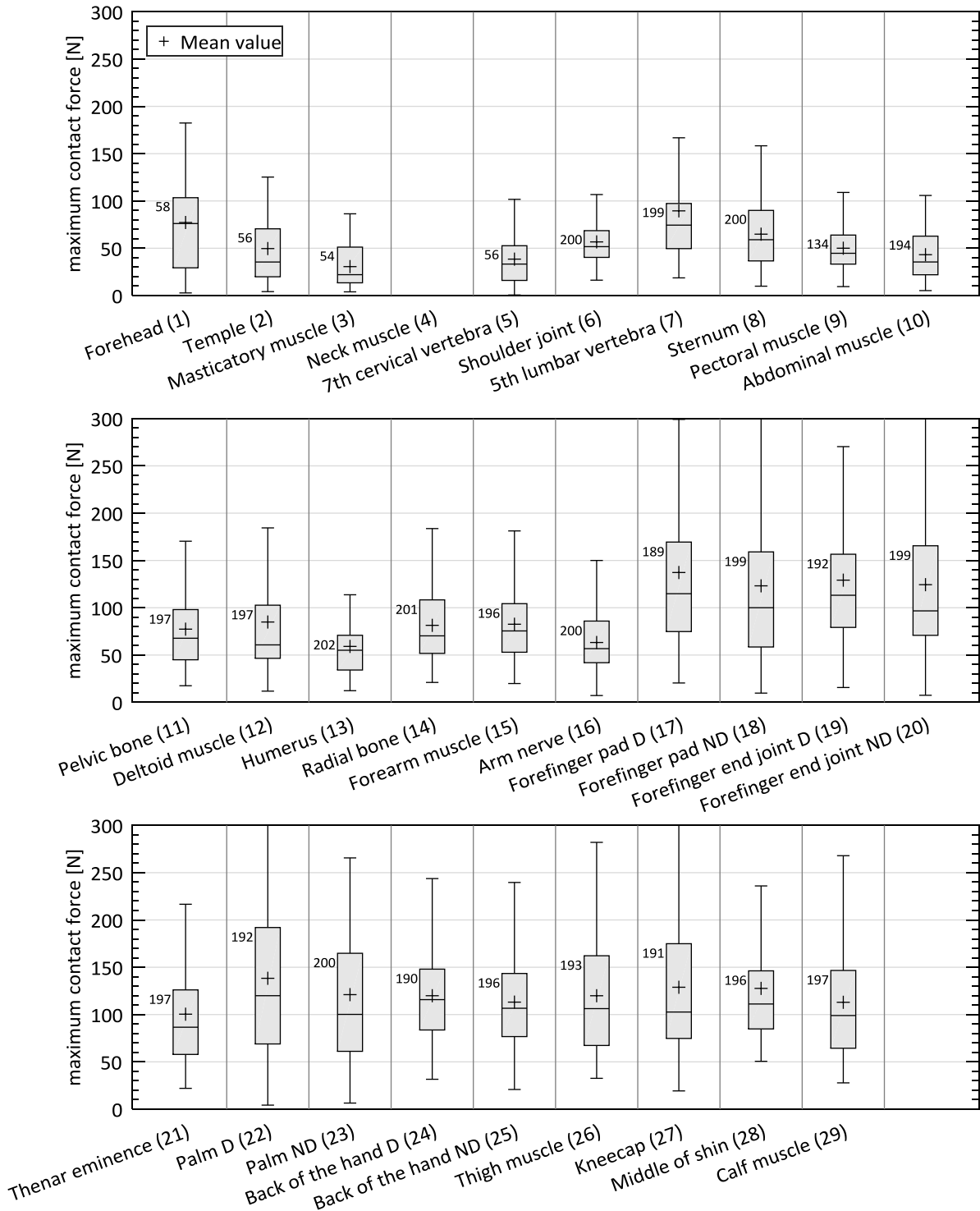


Table 15. Descriptive statistics of transient and semi-sharp contact (transient pressure limits)

Load type		transient (impact)						
Contact type		semi-sharp (pressure-based limits)						
Body part	Body location	Maximum pressure [N/cm ²]						N
		AVG	STD	MIN	MED	MAX	Q3	
Head and neck	(1) Forehead	140.7	97.5	27.1	109.5	570.1	168.9	39
	(2) Temple	58.2	35.3	9.9	47.3	209.8	73.6	39
	(3) Masticatory muscle	42.8	23.4	11.2	41.7	142.2	49.0	39
	(4) Neck muscle	-	-	-	-	-	-	-
	(5) 7th cervical vertebra	138.5	80.8	39.4	121.9	399.1	185.7	39
Trunk	(6) Shoulder joint	90.7	36.9	32.4	82.7	232.4	106.5	77
	(7) 5th lumbar vertebra	158.6	71.3	54.8	150.3	366.5	180.6	43
	(8) Sternum	62.3	28.7	21.9	54.4	125.2	89.1	38
	(9) Pectoral muscle	59.1	23.1	27.8	54.8	114.5	75.3	19
	(10) Abdominal muscle	48.6	24.3	20.4	41.6	117.9	54.2	39
	(11) Pelvic bone	221.7	134.0	28.7	188.9	826.6	283.4	79
Upper extremities	(12) Deltoid muscle	92.9	38.4	38.3	82.8	229.6	112.6	77
	(13) Humerus	116.2	67.9	27.8	97.0	350.7	135.5	77
	(14) Radial bone	142.5	70.4	37.9	138.8	428.5	170.6	79
	(15) Forearm muscle	117.9	49.4	32.7	111.8	359.0	138.3	79
	(16) Arm nerve	111.1	44.1	47.4	104.7	281.8	133.6	79
Hand and fingers	(17) Forefinger pad D	203.3	95.2	42.1	205.5	387.5	244.8	39
	(18) Forefinger pad ND	197.3	97.9	42.2	166.4	471.5	248.3	79
	(19) Forefinger end joint D	499.8	144.5	272.3	466.4	879.9	602.1	39
	(20) Forefinger end joint ND	418.9	168.1	76.7	393.6	814.5	521.7	79
	(21) Thenar eminence	148.9	76.6	51.1	131.4	491.7	179.8	79
	(22) Palm D	270.8	118.4	80.6	268.9	536.9	334.4	39
	(23) Palm ND	242.9	143.7	73.2	196.7	854.3	286.6	78
	(24) Back of the hand D	544.8	264.7	159.9	498.4	1450.9	699.2	39
	(25) Back of the hand ND	381.4	207.2	64.5	335.5	1131.4	471.1	79
Lower extremities	(26) Thigh muscle	136.1	55.7	31.3	127.0	262.6	159.4	79
	(27) Kneecap	225.4	116.4	43.6	202.0	612.4	292.4	77
	(28) Middle of shin	317.5	147.7	48.8	294.2	836.4	413.7	79
	(29) Calf muscle	149.3	73.8	50.8	135.5	378.8	187.0	79

AVG = mean; STD = standard deviation; MIN = minimum; MED = median; MAX = maximum; Q3 = third quartile; N = sample size

Figure 15. Empirical distribution of the data from transient and semi-sharp contact (transient pressure limits)

Load type	transient (impact)
Contact type	semi-sharp (pressure-based limits)

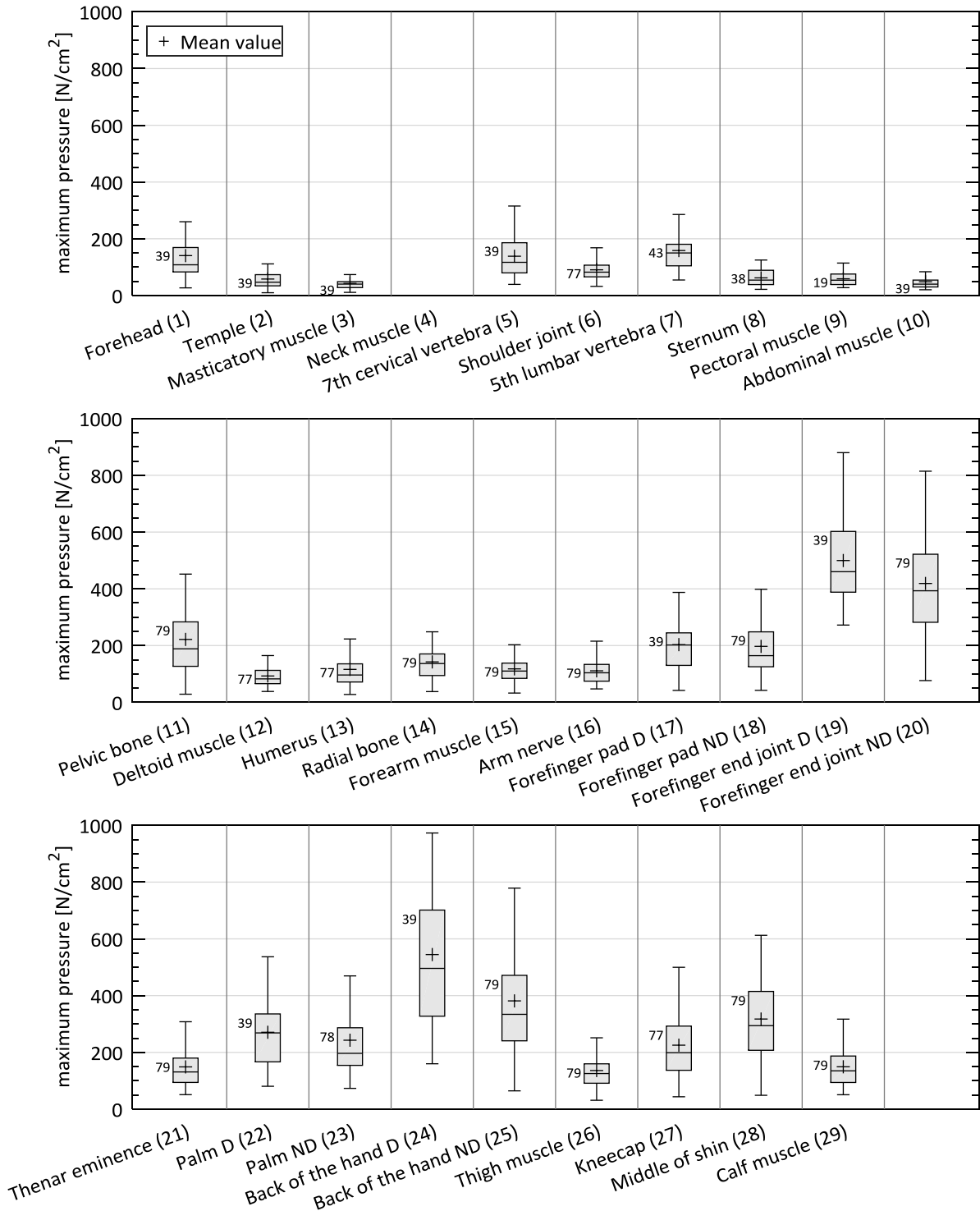


Table 16. Descriptive statistics of transient and semi-sharp contact (maximum contact force)

Load type								
Contact type		semi-sharp						
Body part	Body location	Maximum contact force [N]						N
		AVG	STD	MIN	MED	MAX	Q3	
Head and neck	(1) Forehead	66.7	41.8	9.6	57	202.1	82.7	39
	(2) Temple	41.5	24.3	4.9	38.1	146.7	54.4	39
	(3) Masticatory muscle	36.1	20.3	9.1	33.5	117.2	42.9	39
	(4) Neck muscle	-	-	-	-	-	-	-
	(5) 7th cervical vertebra	48.7	23.2	15.8	42.8	114.3	57.2	39
Trunk	(6) Shoulder joint	55.6	22.6	20.1	54.3	114.2	70.6	77
	(7) 5th lumbar vertebra	133.3	53	54	127.6	268.3	164	43
	(8) Sternum	51	24.9	16	42.8	124.3	69.1	38
	(9) Pectoral muscle	52.9	24.5	20.6	46.3	114.3	62.2	19
	(10) Abdominal muscle	45.3	29.2	11.9	35.7	126.8	49.4	39
	(11) Pelvic bone	105.5	51.4	22.2	96.8	251.5	149	79
Upper extremities	(12) Deltoid muscle	65.8	28.7	14.3	64.9	136.1	88.4	77
	(13) Humerus	82.6	33.2	20.6	82.7	161.8	107.8	77
	(14) Radial bone	96.5	37.7	26.8	95.8	223.5	119.2	79
	(15) Forearm muscle	94	38.4	21.9	88.7	223.4	117.8	79
	(16) Arm nerve	71.9	26.6	27.1	70.2	142.9	89.3	79
Hand and fingers	(17) Forefinger pad D	185.9	67.7	42	181.9	300.7	239.2	39
	(18) Forefinger pad ND	179.2	83.4	31.5	168.9	423.9	224.4	79
	(19) Forefinger end joint D	134.6	55	49.9	136.9	265.3	171	39
	(20) Forefinger end joint ND	132.2	57.5	36	120.2	328.2	165.8	79
	(21) Thenar eminence	120.9	53.4	35.3	115.7	300.6	157.3	79
	(22) Palm D	183.7	64.6	66.7	174.1	321.1	235.2	39
	(23) Palm ND	166.3	73.1	33.1	154.7	351.3	208.2	78
	(24) Back of the hand D	108.5	41	49.2	101.1	230.4	135	39
	(25) Back of the hand ND	87.9	37.5	24.2	85	195.2	113.9	79
Lower extremities	(26) Thigh muscle	122	47.7	20.2	123.9	232.4	148.8	79
	(27) Kneecap	130.6	51.5	35.5	125.9	289.3	171.3	77
	(28) Middle of shin	118	49.2	40.9	117	286.8	155.8	79
	(29) Calf muscle	127.6	57.5	32.4	121.2	259.3	173.2	79

AVG = mean; STD = standard deviation; MIN = minimum; MED = median; MAX = maximum; Q3 = third quartile; N = sample size

Figure 16. Empirical distribution of the data from transient and semi-sharp contact (maximum contact force)

Load type	transient (impact)
Contact type	semi-sharp

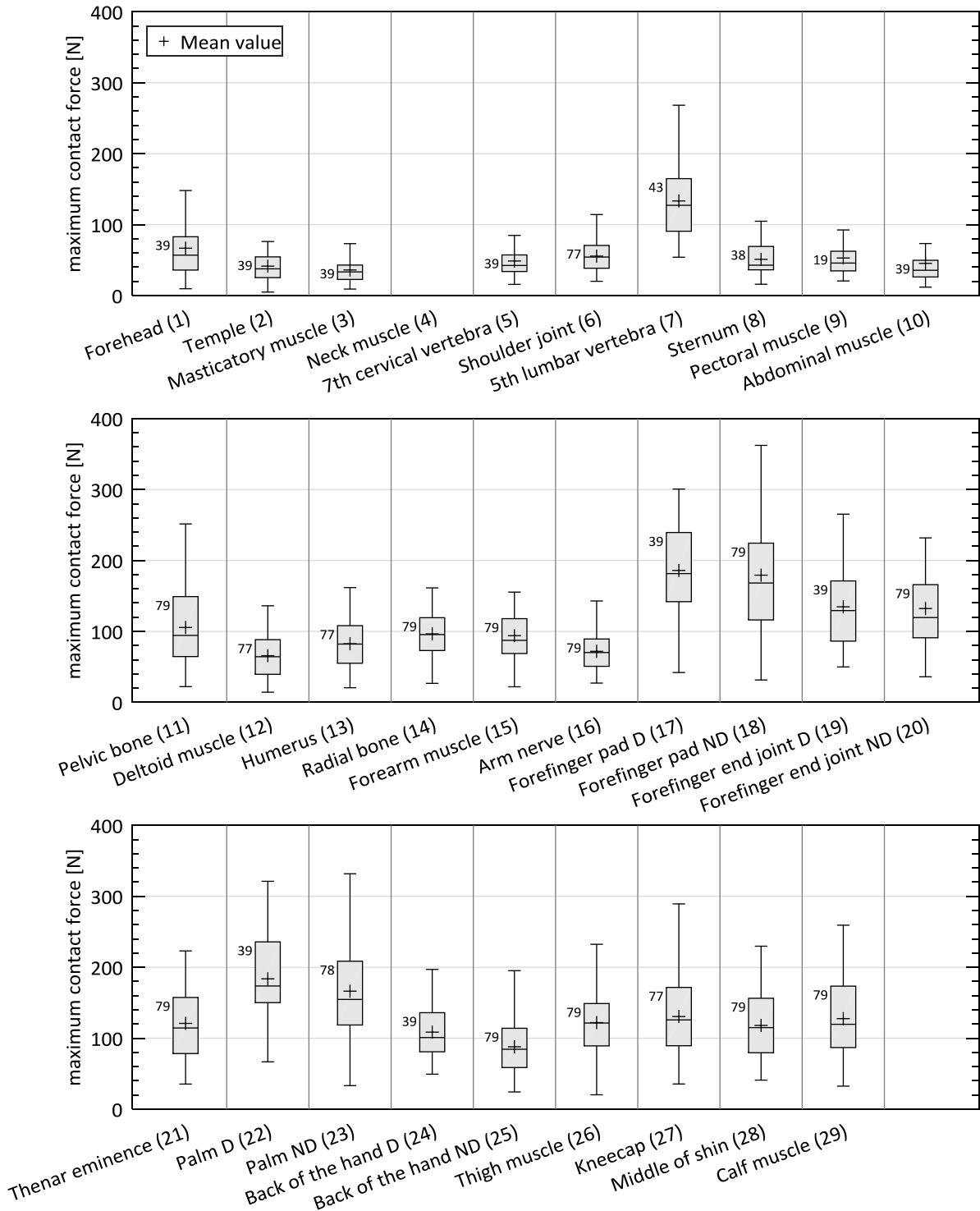


Table 17. Descriptive statistics of transient and semi-sharp contact (maximum deformation)

Load type								
Contact type		semi-sharp						
Body part	Body location	Maximum deformation [mm]						N
		AVG	STD	MIN	MED	MAX	Q3	
Head and neck	(1) Forehead	2.4	0.8	0.8	2.3	4.9	2.9	39
	(2) Temple	6.1	1.6	3.5	5.8	11.5	7.0	39
	(3) Masticatory muscle	11.0	3.2	7.2	10.3	19.6	12.1	39
	(4) Neck muscle	-	-	-	-	-	-	-
	(5) 7th cervical vertebra	13.6	4.2	6.4	13.4	27.2	15.0	39
Trunk	(6) Shoulder joint	17.5	6.7	7.8	15.9	39.4	20.2	77
	(7) 5th lumbar vertebra	15.3	8.3	5.4	13.3	44.5	17.9	43
	(8) Sternum	10.0	3.4	4.7	9.3	18.0	12.3	38
	(9) Pectoral muscle	24.5	6.5	17.6	22.6	44.5	27.9	19
	(10) Abdominal muscle	61.2	17.5	28.4	58.9	97.2	70.0	39
	(11) Pelvic bone	16.6	16.7	1.8	12.1	104.3	18.6	79
Upper extremities	(12) Deltoid muscle	29.8	8.0	14.6	30.1	48.8	35.4	77
	(13) Humerus	14.4	4.8	6.8	13.9	28.9	17.5	77
	(14) Radial bone	11.3	3.7	4.2	10.9	22.9	13.7	79
	(15) Forearm muscle	17.0	3.5	7.7	17.1	24.7	19.1	79
	(16) Arm nerve	17.8	3.9	11.3	17.2	28.2	20.1	79
Hand and fingers	(17) Forefinger pad D	9.1	3.0	3.3	9.2	14.9	11.6	39
	(18) Forefinger pad ND	11.0	5.0	4.0	9.9	33.2	12.7	79
	(19) Forefinger end joint D	5.6	1.6	2.9	5.1	9.1	6.8	39
	(20) Forefinger end joint ND	6.5	2.3	2.5	6.1	13.4	7.4	79
	(21) Thenar eminence	17.7	3.6	9.4	18.0	25.4	20.0	79
	(22) Palm D	11.9	3.2	6.9	11.5	20.6	14.2	39
	(23) Palm ND	14.3	3.2	9.1	13.9	22.7	16.5	78
	(24) Back of the hand D	5.8	1.9	1.9	6.0	11.1	6.7	39
	(25) Back of the hand ND	6.4	2.0	2.8	6.3	14.1	7.2	79
Lower extremities	(26) Thigh muscle	37.3	9.0	22.8	36.2	66.4	40.8	79
	(27) Kneecap	11.0	6.4	2.6	9.1	29.0	13.2	77
	(28) Middle of shin	6.8	3.6	1.6	6.2	20.5	7.9	79
	(29) Calf muscle	34.2	6.7	15.7	34.4	52.5	37.6	79

AVG = mean; STD = standard deviation; MIN = minimum; MED = median; MAX = maximum; Q3 = third quartile; N = sample size

Figure 17. Empirical distribution of the data from quasi-static and semi-sharp contact (maximum deformation; control group)

Load type	transient (impact)
Contact type	semi-sharp

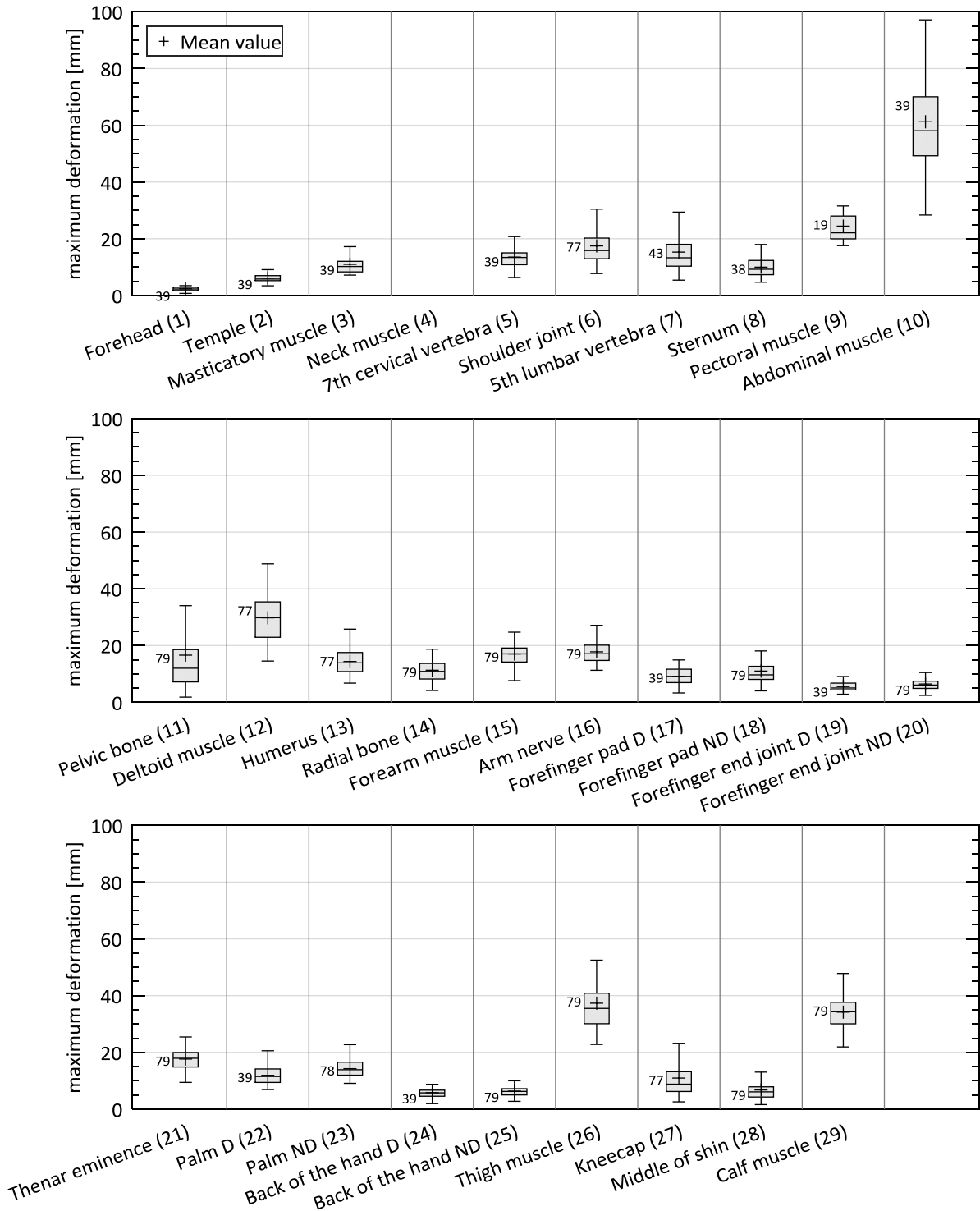


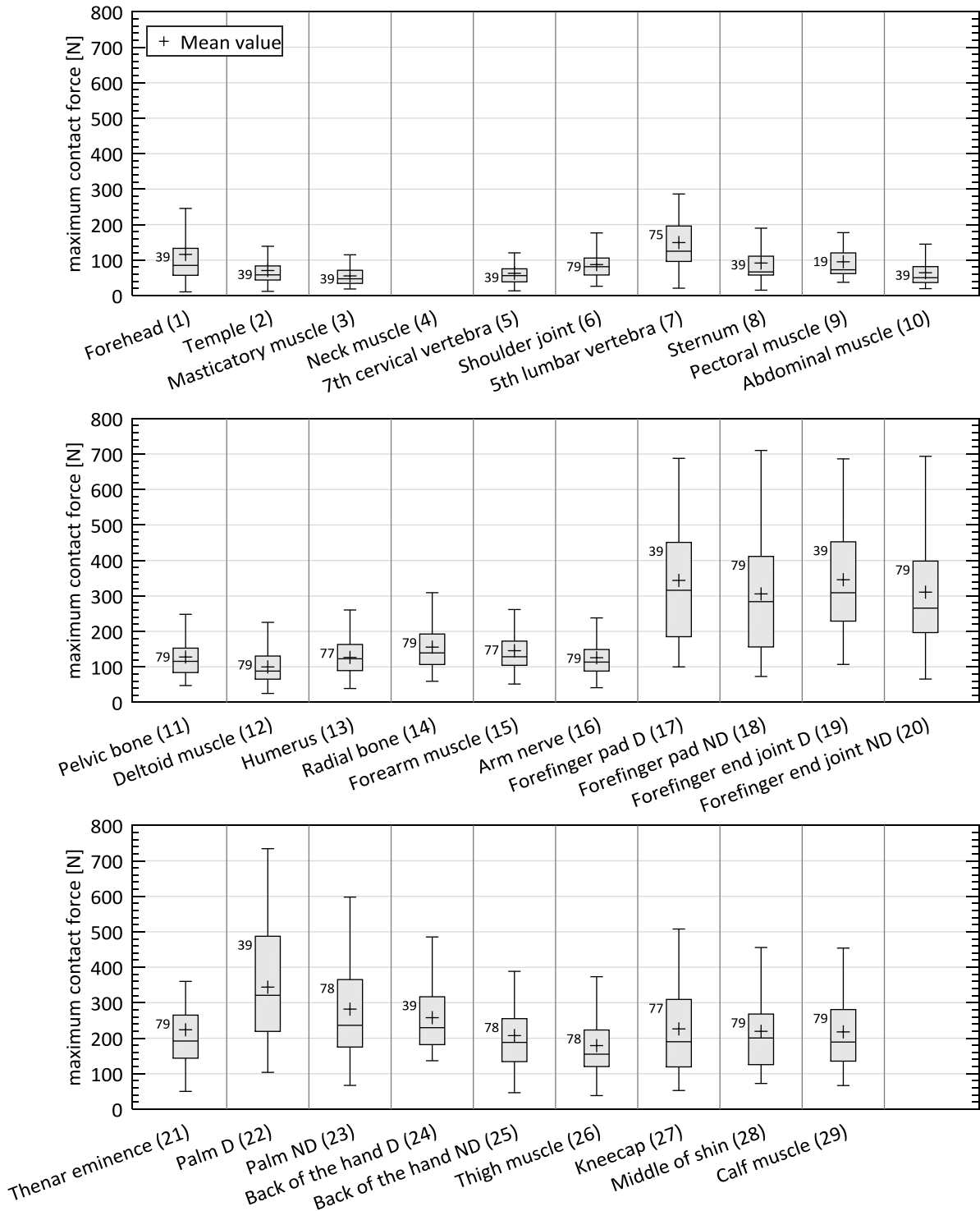
Table 18. Descriptive statistics of transient and blunt contact (transient force limits)

Load type	transient (impact)							
Contact type	blunt (force-based limits)							
Body part	Body location	Maximum force [N]						N
		AVG	STD	MIN	MED	MAX	Q3	
Head and neck	(1) Forehead	116.0	99.8	10.4	85.2	485.5	132.8	39
	(2) Temple	70.6	45.2	11.8	59.1	211.5	83.5	39
	(3) Masticatory muscle	55.4	29.0	18.6	48.2	140.8	70.6	39
	(4) Neck muscle	-	-	-	-	-	-	-
	(5) 7th cervical vertebra	62.7	33.4	13.3	56.7	174.6	75.3	39
Trunk	(6) Shoulder joint	87.2	39.0	26.2	81.4	198.9	105.4	79
	(7) 5th lumbar vertebra	149.3	78.5	20.7	125.0	412.7	195.7	75
	(8) Sternum	91.6	61.8	15.1	67.8	239.7	110.7	39
	(9) Pectoral muscle	95.1	50.6	37.4	79.4	220.2	120.0	19
	(10) Abdominal muscle	64.3	40.1	19.4	50.8	182.6	81.5	39
	(11) Pelvic bone	127.8	61.2	47.4	115.8	380.7	152.6	79
Upper extremities	(12) Deltoid muscle	99.8	47.9	25.1	88.1	231.7	130.4	79
	(13) Humerus	126.8	47.7	39.1	123.5	260.4	163.0	77
	(14) Radial bone	155.6	75.6	59.4	140.4	481.1	192.6	79
	(15) Forearm muscle	145.6	64.2	51.6	130.3	345.4	172.5	77
	(16) Arm nerve	125.8	58.1	41.3	114.8	341.8	148.9	79
Hand and fingers	(17) Forefinger pad D	343.8	178.3	100.0	325.3	687.9	448.5	39
	(18) Forefinger pad ND	305.7	171.6	72.9	290.9	710.1	410.9	79
	(19) Forefinger end joint D	345.7	150.7	106.9	313.0	686.5	450.7	39
	(20) Forefinger end joint ND	310.6	159.4	65.6	267.8	740.1	397.7	79
	(21) Thenar eminence	223.7	120.9	50.0	192.3	639.4	264.9	79
	(22) Palm D	343.9	162.9	103.7	326.3	734.3	482.0	39
	(23) Palm ND	282.0	148.2	66.9	236.4	768.3	364.2	78
	(24) Back of the hand D	257.8	97.9	136.5	243.1	485.4	316.2	39
	(25) Back of the hand ND	207.3	101.4	46.4	188.2	583.6	253.3	78
Lower extremities	(26) Thigh muscle	179.2	93.7	38.2	154.9	533.6	223.1	78
	(27) Kneecap	226.2	129.2	52.6	190.1	645.5	308.9	77
	(28) Middle of shin	219.4	113.3	72.4	202.2	665.4	267.8	79
	(29) Calf muscle	217.8	107.8	66.5	189.4	609.6	280.6	79

AVG = mean; STD = standard deviation; MIN = minimum; MED = median; MAX = maximum; Q3 = third quartile; N = sample size

Figure 18. Empirical distribution of the data from transient and blunt contact (transient force limits)

Load type	transient (impact)
Contact type	blunt (force-based limits)



5.4.3 Hypothesis testing

In Section 2.1, we hypothesized that the contact period and the contact area influence the pain thresholds' trend. This section will demonstrate whether our hypotheses are correct, albeit the descriptive statistics have already proven they are. We must rephrase the hypotheses for the test so that the test can disprove their antitheses. Observations have to be based on the same output variables so that the hypotheses for the blunt and semi-sharp contact bodies can be tested equally. Another requirement is that the observations analyzed by the test rely all on the same output variable. We will use the maximum contact force since it is the only output variable that we measured in every test.

Since the samples from our studies are incomplete (one subject did not finish the study for instance), we cannot use standard methods such as repeated-measures ANOVA to disprove both hypotheses. A linear mixed model constitutes a suitable method for obtaining reliable evidence even from imperfect samples. This statistical model analyzes the observations \tilde{z}_i from subject i as a linear combination of explanatory variables \mathbf{x}_i^T with fixed effects $\boldsymbol{\beta}$ and additional explanatory variables \mathbf{u}_i^T with random and subject-specific effects $\boldsymbol{\gamma}$ (Fahrmeir et al. 2009)

$$\tilde{z}_i = \mathbf{x}_i^T \boldsymbol{\beta} + \mathbf{u}_i^T \boldsymbol{\gamma} + \varepsilon_i \quad .$$

In our rephrased hypotheses, the explanatory variable consists of the nominal variable x_{Li} representing the load type and x_{Si} representing the contact body type

$$\mathbf{x}_i^T = [1 \quad x_{Li} \quad x_{Si}] \quad .$$

Table 19 presents the values we assigned to both nominal-scaled variables. Next, we need to find a transformation that ensures the observations \tilde{z}_i are distributed normally, a requirement for the linear mixed model. Since an Anderson-Darling test demonstrated that the log-normal distribution represents the form of the empirical cumulative distribution most accurately, we applied the following transformation to convert the observations, thus meeting the requirements

$$\tilde{z}_i = \ln z_i \quad .$$

Table 19. Values of the nominal-scale explanatory variables for hypothesis testing

Load type	Contact type	x_L	x_S
Quasi-static	Semi-sharp	1	1
	Blunt	1	2
Transient	Semi-sharp	2	1
	Blunt	2	2

Once \tilde{z}_i and \mathbf{x}_i^T are in place, we can refine the regression model as follows

$$\ln z_i = \mathbf{x}_i^T \boldsymbol{\beta} + \gamma_{i0} + \varepsilon_i$$

where γ_{i0} is the subject-specific variance. We used the MATLAB function `fitlme` to determine the fixed effects $\boldsymbol{\beta}$ of the model. If $\beta_k = \boldsymbol{\beta}$ differ significantly from zero $\beta_k \neq 0$, the test disproves the hypothesis linked with the slope factor $k \in \{0,1,2\}$

$$H_0: \beta_k = 0 \quad \text{the covariable has no influence}$$

$$H_1: \beta_k \neq 0 \quad \text{the covariable has an influence}$$

In our case, $\beta_k \neq 0$ indicates that the covariable x_k affects pain thresholds. The Wilkinson notation for the MATLAB function `fitlme` is

$$\text{force} \sim \text{studyID} + \text{shapeID} + (1 \mid \text{subjectID})$$

We used a significance level of $\alpha = 0.05$. Table 20 presents the test results in order of body location. As columns 6 and 8 show, the p value is always $p \leq \alpha$, indicating the test disproves both hypotheses. The test thus delivers strong evidence that load type and contact body type influence pain threshold trends.

Table 20. Results of the hypotheses test

Body part	Body location	β_0	p	Load type		Contact type	
				β_1	p	β_2	p
Head and neck	(1) Forehead	2.109	<0.001	0.568	<0.001	0.620	<0.001
	(2) Temple	1.871	<0.001	0.475	<0.001	0.624	<0.001
	(3) Masticatory muscle	1.597	<0.001	0.440	<0.001	0.695	<0.001
	(4) Neck muscle	-	-	-	-	-	-
	(5) 7th cervical vertebra	1.605	<0.001	0.385	0.010	0.861	<0.001
Trunk	(6) Shoulder joint	2.694	<0.001	0.386	<0.001	0.405	<0.001
	(7) 5th lumbar vertebra	2.972	<0.001	0.257	<0.001	0.659	<0.001
	(8) Sternum	2.426	<0.001	0.455	<0.001	0.575	<0.001
	(9) Pectoral muscle	2.441	<0.001	0.508	<0.001	0.405	<0.001
	(10) Abdominal muscle	2.122	<0.001	0.291	<0.001	0.752	<0.001
	(11) Pelvic bone	3.045	<0.001	0.205	<0.001	0.619	<0.001
Upper extremities	(12) Deltoid muscle	3.106	<0.001	0.356	<0.001	0.291	<0.001
	(13) Humerus	1.831	<0.001	0.554	<0.001	0.932	<0.001
	(14) Radial bone	2.544	<0.001	0.511	<0.001	0.668	<0.001
	(15) Forearm muscle	2.672	<0.001	0.455	<0.001	0.611	<0.001
	(16) Arm nerve	2.172	<0.001	0.529	<0.001	0.706	<0.001
Hand and fingers	(17) Forefinger pad D	2.714	<0.001	0.536	<0.001	0.880	<0.001
	(18) Forefinger pad ND	2.495	<0.001	0.509	<0.001	0.990	<0.001
	(19) Forefinger end joint D	1.713	<0.001	0.995	<0.001	0.966	<0.001
	(20) Forefinger end joint ND	2.078	<0.001	0.800	<0.001	0.909	<0.001
	(21) Thenar eminence	2.320	<0.001	0.607	<0.001	0.825	<0.001
	(22) Palm D	2.411	<0.001	0.641	<0.001	0.954	<0.001
	(23) Palm ND	2.391	<0.001	0.538	<0.001	0.997	<0.001
	(24) Back of the hand D	2.022	<0.001	0.926	<0.001	0.761	<0.001
	(25) Back of the hand ND	2.124	<0.001	0.889	<0.001	0.633	<0.001
Lower extremities	(26) Thigh muscle	3.435	<0.001	0.317	<0.001	0.444	<0.001
	(27) Kneecap	3.194	<0.001	0.415	<0.001	0.569	<0.001
	(28) Middle of shin	3.004	<0.001	0.543	<0.001	0.515	<0.001
	(29) Calf muscle	2.751	<0.001	0.521	<0.001	0.684	<0.001

6 Discussion

Most standards use data from experiments and extensive literature surveys to define biomechanical limits. This wide range of sources often contribute heterogeneous data to the limits (Behrens et al. 2014). This study was intended to define limits for all pertinent body locations based on homogenous and consistent data from one particular source, regardless of whether sources or data that already fit to the study's objective are available.

6.1 Comparison of the data

As the work plan indicates, one of our final study's objectives was the testing of a control group with the same parameters Johannes Gutenberg University Mainz (JGU) used in 2014 to determine pressure-based limits for quasi-static and semi-sharp contacts. This control group was intended to ensure that our study protocol and procedures produced results comparable to those obtained by JGU.

Figure 19 compares the pressure-based pain thresholds from the Fraunhofer IFF's control group with those from the over 100 subjects in JGU's study. We received the data from the IFA by courtesy. The box plots reveal a noticeable difference between both studies. The pain thresholds from JGU exceed those from the Fraunhofer IFF for most body locations, especially for body parts with distinct soft tissue layers covering bone. A comparison of the pain thresholds based on maximum contact forces paints an entirely different picture (Figure 20, page 45). The means of these box plots reveal a significantly smaller difference than the means of the pressure-based thresholds in Figure 19 have. Should this study protocol differ completely from JGU's study protocol, the force-based thresholds ought to deviate similarly to the pressure-based thresholds. While JGU conceivably may have based their analysis on a different approach, a South Korean study completed in 2019 with results similar to ours arrived at the same conclusions.

Figure 19. Comparison of the maximum pressures from the Fraunhofer IFF's control group and the study of JGU Mainz

Load type	quasi-static (clamping)
Contact body type	semi-sharp

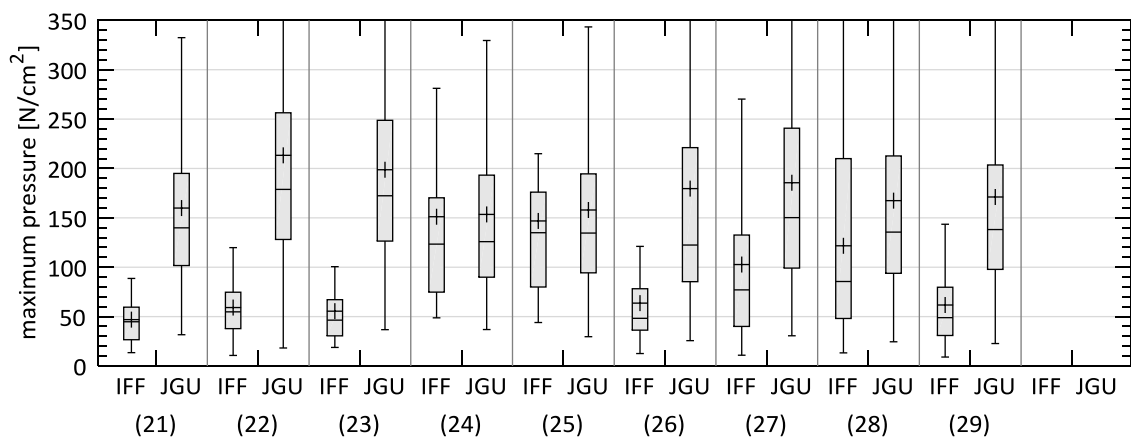
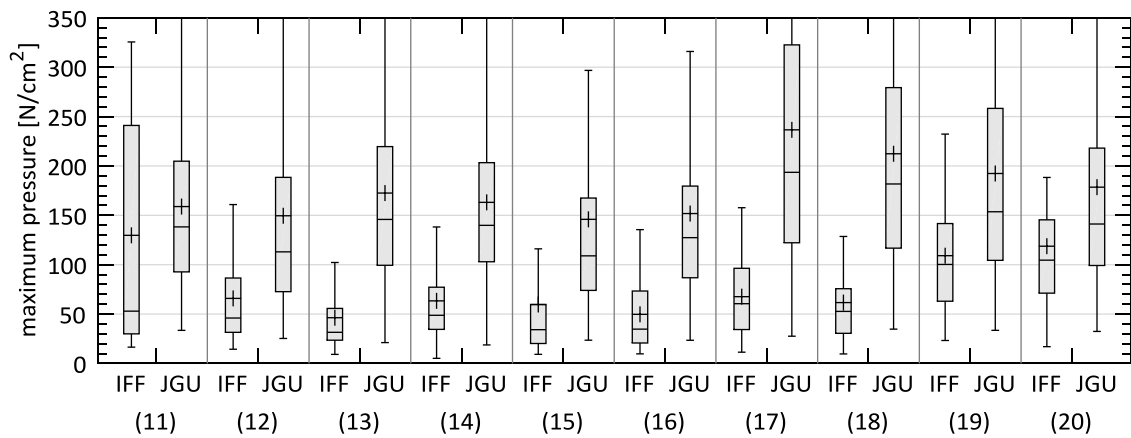
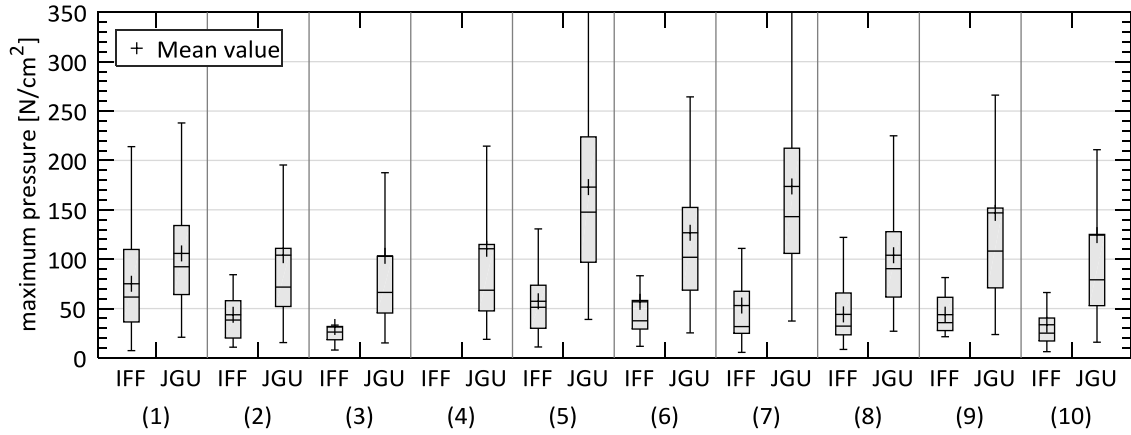
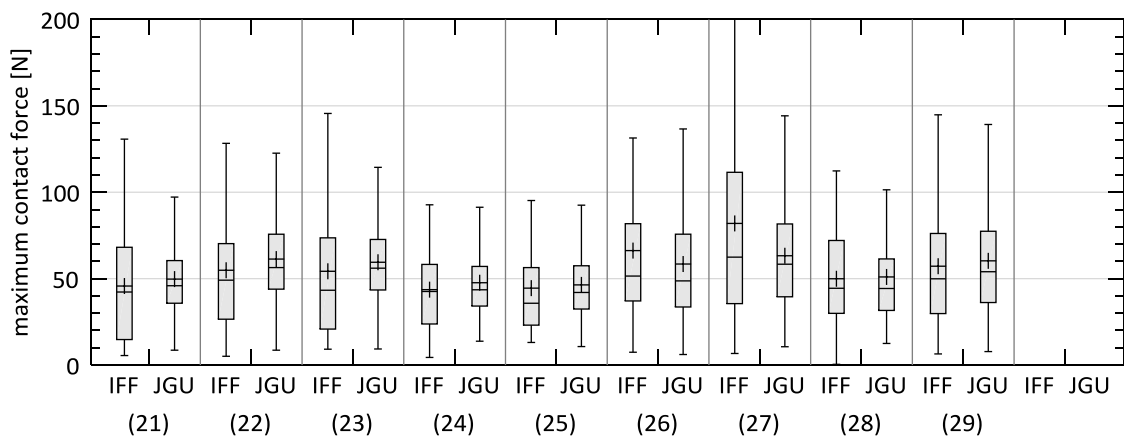
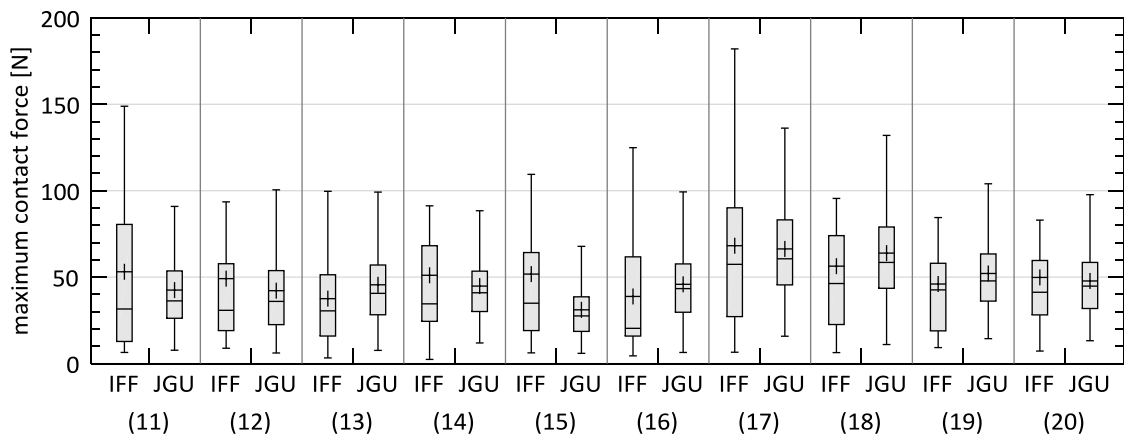
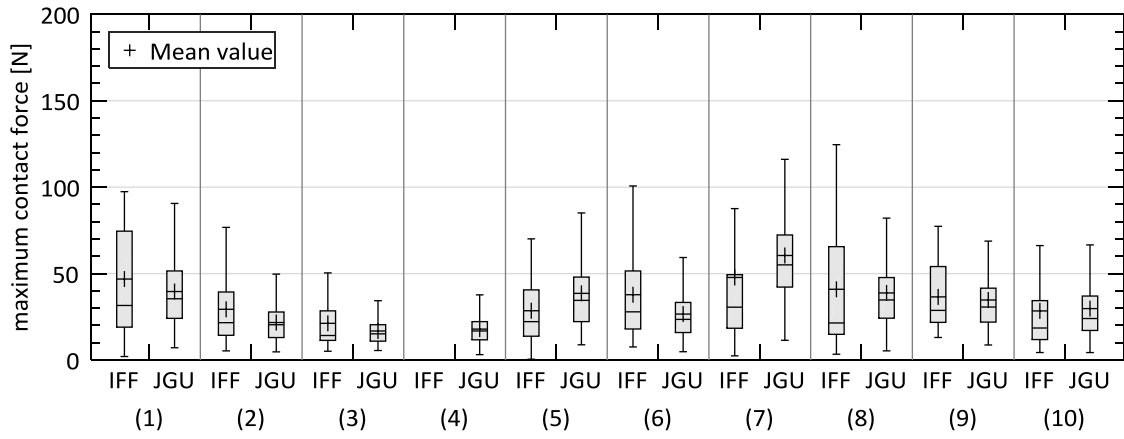


Figure 20. Comparison of the maximum force from the Fraunhofer IFF's control group and the study of JGU Mainz

Load type	quasi-static (clamping)
Contact body type	semi-sharp



6.2 Limit values

FBHM 080 and ISO/TS 15066 identify the 3rd quartile of the empirically distributed thresholds as the desired limit value for the corresponding body location and contact type. Column 8 of Table 14 through 18 contains the 3rd quartile of the pressure- and force-based pain thresholds for all body locations and contact types tested. Extracting the 3rd quartile values and rounding them to their last digit yields the results presented in Table 21. We also include ISO/TS 15066's pressure-based limits for quasi-static contact from the JGU in the column 3 of Table 21, even though section 6.1 represents a substantial deviation from our results,.

The last two columns of Table 21 contain factors that convert the quasi-static limits into transient limits

$$\hat{\psi}_{TR} = V_{\psi}\hat{\psi}_{QS} \quad \hat{F}_{TR} = V_{\psi}F_{QS} \quad .$$

Since we could not perform any load tests on (4) neck muscle (see Section 2.3.1), we had to estimate its limits. The individual force-based thresholds provided by JGU for (3) masticatory muscle and (4) neck muscle are distributed equally (see Figure 20). We can therefore assume that the desired limit for (4) neck muscle is close to that for (3) masticatory muscle. The means of both samples reveal that the threshold for (4) neck muscle is 1.1 times the threshold for (3) masticatory muscle. Applying this relative difference to the limits of (3) masticatory muscle yields the estimations for (4) neck muscle.

Table 22 contains the results from our control group rather than JGU's group of 100 subjects, thus resulting in different factors for pressure limit conversion. Since we do not believe that the limits from JGU represent individuals' actual pain thresholds, we strongly recommend that the limits in Table 22 for future revisions and publications of standards.

Table 21. Limit values, including those provided by JGU for FBHM 080 and ISO/TS 15066

Body part	Body location	Quasi-static (QS)		Transient (TR)		Factors QS → TR	
		ψ_{QS} [N/cm ²]	F_{QS} [N]	ψ_{TR} [N/cm ²]	F_{TR} [N]	V_{ψ}	V_F
Head and neck	(1) Forehead	130	100	170	130	1.3	1.3
	(2) Temple	110	70	70	80	0.6	1.1
	(3) Masticatory muscle	110	50	50	70	0.5	1.4
	(4) Neck muscle	140	60*	60*	80*	0.4	1.3
	(5) 7th cervical vertebra	210	50	190	80	0.9	1.6
Trunk	(6) Shoulder joint	160	70	110	110	0.7	1.6
	(7) 5th lumbar vertebra	210	100	180	200	0.9	2.0
	(8) Sternum	120	90	90	110	0.8	1.2
	(9) Pectoral muscle	170	60	80	120	0.5	2.0
	(10) Abdominal muscle	140	60	50	80	0.4	1.3
	(11) Pelvic bone	210	100	280	150	1.3	1.5
Upper extremities	(12) Deltoid muscle	190	100	110	130	0.6	1.3
	(13) Humerus	220	70	140	160	0.6	2.3
	(14) Radial bone	180	110	170	190	0.9	1.7
	(15) Forearm muscle	190	100	140	170	0.7	1.7
	(16) Arm nerve	180	90	130	150	0.7	1.7
Hand and fingers	(17) Forefinger pad D	300	170	240	450	0.8	2.6
	(18) Forefinger pad ND	270	160	250	410	0.9	2.6
	(19) Forefinger end joint D	280	160	600	450	2.1	2.8
	(20) Forefinger end joint ND	220	170	520	400	2.4	2.4
	(21) Thenar eminence	200	130	180	260	0.9	2.0
	(22) Palm D	260	190	330	480	1.3	2.5
	(23) Palm ND	260	160	290	360	1.1	2.3
	(24) Back of the hand D	200	150	700	320	3.5	2.1
	(25) Back of the hand ND	190	140	470	250	2.5	1.8
Lower extremities	(26) Thigh muscle	250	160	160	220	0.6	1.4
	(27) Kneecap	220	170	290	310	1.3	1.8
	(28) Middle of shin	220	150	410	270	1.9	1.8
	(29) Calf muscle	210	150	190	280	0.9	1.9

*) estimated

Table 22. Limit values, including those from the control group of this study

Body part	Body location	Quasi-static (QS)		Transient (TR)		Factors QS → TR	
		ψ_{QS} [N/cm ²]	F_{QS} [N]	ψ_{TR} [N/cm ²]	F_{TR} [N]	V_{ψ}	V_F
Head and neck	(1) Forehead	110	100	170	130	1.5	1.3
	(2) Temple	60	70	70	80	1.2	1.1
	(3) Masticatory muscle	30	50	50	70	1.7	1.4
	(4) Neck muscle	30*	60*	60*	80*	2.0	1.3
	(5) 7th cervical vertebra	70	50	190	80	2.7	1.6
Trunk	(6) Shoulder joint	60	70	110	110	1.8	1.6
	(7) 5th lumbar vertebra	70	100	180	200	2.6	2.0
	(8) Sternum	70	90	90	110	1.3	1.2
	(9) Pectoral muscle	60	60	80	120	1.3	2.0
	(10) Abdominal muscle	40	60	50	80	1.3	1.3
	(11) Pelvic bone	240	100	280	150	1.2	1.5
Upper extremities	(12) Deltoid muscle	90	100	110	130	1.2	1.3
	(13) Humerus	60	70	140	160	2.3	2.3
	(14) Radial bone	80	110	170	190	2.1	1.7
	(15) Forearm muscle	60	100	140	170	2.3	1.7
	(16) Arm nerve	70	90	130	150	1.9	1.7
Hand and fingers	(17) Forefinger pad D	100	170	240	450	2.4	2.6
	(18) Forefinger pad ND	80	160	250	410	3.1	2.6
	(19) Forefinger end joint D	140	160	600	450	4.3	2.8
	(20) Forefinger end joint ND	150	170	520	400	3.5	2.4
	(21) Thenar eminence	60	130	180	260	3.0	2.0
	(22) Palm D	70	190	330	480	4.7	2.5
	(23) Palm ND	70	160	290	360	4.1	2.3
	(24) Back of the hand D	170	150	700	320	4.1	2.1
	(25) Back of the hand ND	180	140	470	250	2.6	1.8
Lower extremities	(26) Thigh muscle	80	160	160	220	2.0	1.4
	(27) Kneecap	130	170	290	310	2.2	1.8
	(28) Middle of shin	210	150	410	270	2.0	1.8
	(29) Calf muscle	80	150	190	280	2.4	1.9

*) estimated

7 References

- Arthur, R. P.; Shelly, W. B. (1959): The innervation of human epidermis. In: *The Journal of investigative dermatology* 32 (3), S. 397–411. Online verfügbar unter <http://worldcatlibraries.org/wcpa/oclc/102914863>.
- Behrens, R.; Lerez, C.; Elkmann, N.; Jachau, K.; Schmidt, S. (2014): KAN-Studie 52: Biomechanische Belastungsgrenzen. Abschlussbericht. Hg. v. KAN - Kommission Arbeitsschutz und Normung.
- Besne, I.; Descombes, C.; Breton, L. (2002): Effect of Age and Anatomical Site on Density of Sensory Innervation in Human Epidermis. In: *Archives of Dermatology* 138, S. 1445–1453. Online verfügbar unter <http://worldcatlibraries.org/wcpa/oclc/201334214>.
- Bishop, R. F. (1945): The theory of indentation and hardness tests. In: *Proceedings of the Physical Society* 57 (3), S. 147–159. Online verfügbar unter urn:ISSN:0959-5309.
- Fahrmeir, L.; Kneib, T.; Lang, S. (2009): Regression. Modelle, Methoden und Anwendungen. Berlin: Springer. Online verfügbar unter <http://worldcatlibraries.org/wcpa/oclc/680613388>.
- IFA (2009): BG/BGIA risk assessment recommendations according to machinery directive: Design of workplaces with collaborative robots, zuletzt aktualisiert am February 2011, zuletzt geprüft am 22.08.2013.
- Isselee, H.; Laat, A. de; Lesaffre, E.; Lysens, R. (1997): Short-term reproducibility of pressure pain thresholds in masseter and temporalis muscles of symptom-free subjects. In: *European journal of oral sciences* 105 (6), S. 583–587.
- Lauria, G.; Holland, N.; Hauer, P.; Cornblath, D. R.; Griffin, J. W.; McArthur, J. C. (1999): Epidermal innervation: changes with aging, topographic location, and in sensory neuropathy. In: *Journal of the neurological sciences* 164 (2), S. 172–178. Online verfügbar unter <http://worldcatlibraries.org/wcpa/oclc/120874686>.
- List, T.; Helkimo, M.; Karlsson, R. (1991): Influence of pressure rates on the reliability of a pressure threshold meter. In: *Journal of craniomandibular disorders : facial & oral pain* 5 (3), S. 173–178. Online verfügbar unter <http://worldcatlibraries.org/wcpa/oclc/118201923>.
- Nahum, A. M.; Gadd, C. W.; Schneider, D. C.; Madeira, R. G. (1972): Tolerances of superficial soft tissues to injury. In: *Journal of trauma* 12 (12), S. 1044–1052.
- Povse, B.; Koritnik, D.; Kamnik, R.; Bajd, T.; Munih, M. (2010a): Cooperation of human operator and small industrial robot. In: *International journal automation Austria* 18 (1), S. 80–86. Online verfügbar unter <http://worldcatlibraries.org/wcpa/oclc/781072681>.
- Povse, B.; Koritnik, D.; Kamnik, R.; Bajd, T.; Munih, M. (2011): Emulation system for assessment of human-robot collision. In: *Meccanica* 46 (6), S. 1363–1371. Online verfügbar unter <http://worldcatlibraries.org/wcpa/oclc/767588006>.
- Povse, B.; Koritnik, D.; Kamnik, R.; Bajd, T.; Munih, M. (2010b): Industrial robot and human operator collision. In: *Proceedings of the 2010 IEEE International Conference on Systems Man and Cybernetics*, S. 2663–2668. DOI: 10.1109/ICSMC.2010.5641897.

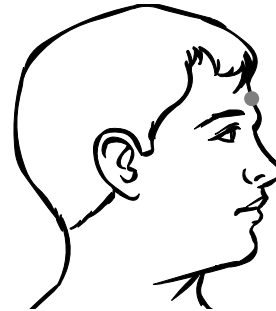
- Saito, T.; Ikeda, H. (2005): Measurement of Human Pain Tolerance to Mechanical Stimulus of Human-collaborative Robots. In: *Specific Research Reports of the National Institute of Industrial Safety* 33, S. 16–23.
- Sarlani, E.; Greenspan, J. D. (2002): Gender differences in temporal summation of mechanically evoked pain. In: *PA/W* 97 (1-2), S. 163–169. Online verfügbar unter <http://worldcatlibraries.org/wcpa/oclc/111337799>.
- Stalnaker, R. L.; Melvin, J. W. (1976): Human tolerance to lower extremities impacts. In: *Proceedings of the Meeting on Biomechanics of Injury to Pedestrians, Cyclists and Motorcyclists*, S. 362–374. Online verfügbar unter <http://worldcatlibraries.org/wcpa/oclc/55138303>.
- Sun, J. (2006): *The Statistical Analysis of Interval-censored Failure Time Data*. 1. Aufl. New York: Springer. Online verfügbar unter <http://worldcatlibraries.org/wcpa/oclc/990546944>.
- Takala, E. P. (1990): Pressure pain threshold on upper trapezius and levator scapulae muscles. Repeatability and relation to subjective symptoms in a working population. In: *Scandinavian journal of rehabilitation medicine* 22 (2), S. 63–68. Online verfügbar unter <http://worldcatlibraries.org/wcpa/oclc/121651853>.
- Vierck, C. J.; Cannon, R. L.; Fry, G.; Maixner, W.; Whitsel, B. L. (1997): Characteristics of temporal summation of second pain sensations elicited by brief contact of glabrous skin by a preheated thermode. In: *Journal of neurophysiology* 78 (2), S. 992–1002.
- Yamada, Y. (1997): Evaluation of Human Pain Tolerance and Its Application to Designing Safety Robot Mechanisms for Human-Robot Coexistence. In: *Journal of Robotics and Mechatronics* 9 (1), S. 65–70. Online verfügbar unter <http://worldcatlibraries.org/wcpa/oclc/199841232>.
- Yamada, Y.; Suita, K.; Ikeda, H.; Sugimoto, N.; Miura, H.; Nakamura, H. (1997): Evaluation of Pain Tolerance Based on a Biomechanical Method for Human-Robot Coexistence. In: *Transactions of the Japan Society of Mechanical Engineers Series C* 63 (612), S. 2814–2819. Online verfügbar unter <http://worldcatlibraries.org/wcpa/oclc/4815102968>.
- Yamada, Y.; Suita, K.; Imai, K.; Ikeda, H.; Sugimoto, N. (1996): A failure-to-safety robot system for human-robot coexistence. In: *Robotics and Autonomous Systems* 18 (1), S. 283–291. Online verfügbar unter <http://worldcatlibraries.org/wcpa/oclc/4930888155>.

A Body Locations

The following list describes the anatomical landmarks and distances we used to localize the body locations tested.

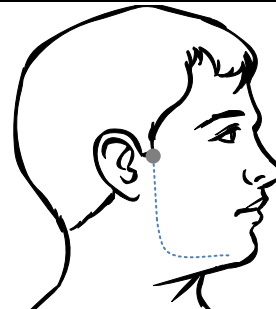
(1) Forehead

The contact point is centered on the forehead in a distance of a thumb-space from the glabella.



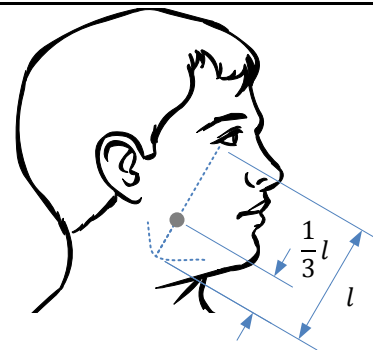
(2) Temple

The contact point is on the line running cranially along the rear edge of the mandibular ramus in cranial direction. The point has a distance of a thumb-space from the level of the tragus.



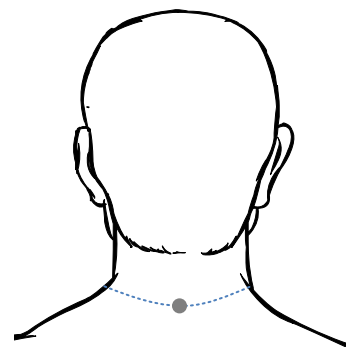
(3) Masticatory muscle

The contact point is on the line running from the outermost point of the mandibular ramus toward the eye. Its distance from the outermost point of the mandibular ramus is one-third of the line's total length.



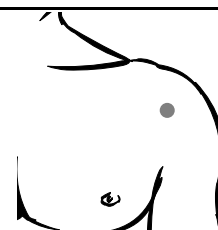
(5) 7th cervical vertebra

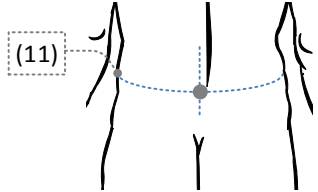
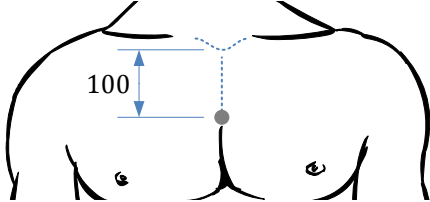
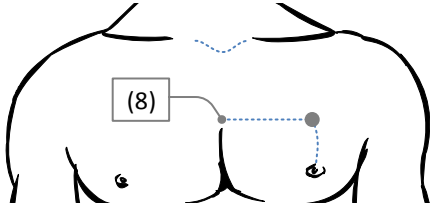
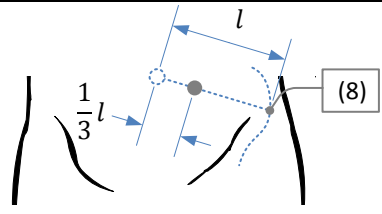
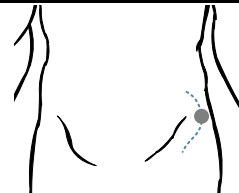
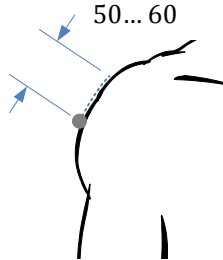
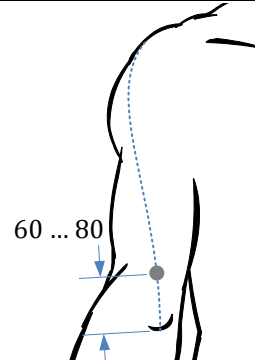
The contact point is the outermost posterior point of the 7th cervical vertebra.



(6) shoulder joint

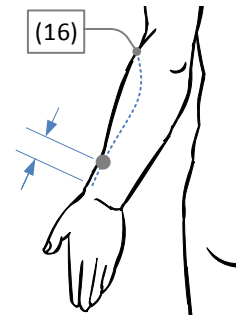
The contact point is the outermost point anterior to the spherical shoulder joint.



(7) 5th lumbar vertebra	The contact point is the outermost posterior point of the 5th lumbar vertebra (L5). L5 is approximately on the same level as contact point (11).	
(8) Sternum	The contact point is on the middle line of the thorax running in caudal direction. Its distance from the jugular notch in caudal direction is 100 mm.	
(9) Pectoral muscle	The contact point is the intersection point of the line from (8) in lateral direction with the line from the nipple on the non-dominant body side in cranial direction.	
(10) Abdominal muscle	The contact point is on the line running from (8) toward the navel. Its distance from the navel is one-third of the line's total length.	
(11) Pelvic bone	The contact point is the outermost anterior point of the iliac crest.	
(12) Deltoid muscle	The contact point lies in the lateral middle line of the upper arm. Its distance from the acromion is 50 to 60 mm (depending on the length of the humerus).	
(13) Humerus	The contact point is on virtual line running from the acromion to the upper end of the elbow joint. Its cranial distance from the elbow joint is 60 to 80 mm (depending on the length of the humerus).	

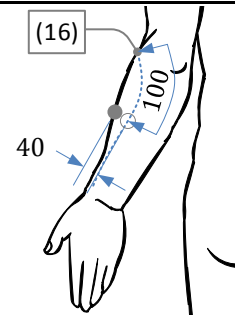
(14) Radial bone

The contact point is on the line running from the outermost lateral point of the triquetral bone to (16). Its cranial distance from the triquetral bone is 40 mm.



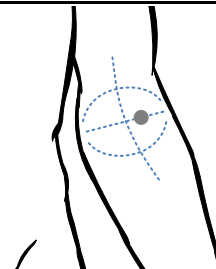
(15) Forearm muscle

The contact point lies a lateral distance of 40 mm from the supporting point, which is on the line running from (16) to the outermost lateral point of the triquetral bone. The distance of the supporting point from (16) is 100 mm.



(16) Elbow pit

The contact point is on the middle skin fold of the elbow pit, which appears when the arm is slightly bent. Its lateral distance from the biceps tendon is 10 mm.

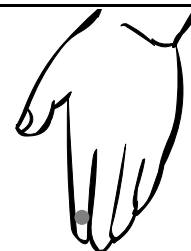


(17)/(18) Forefinger pad

The contact point is in the center of the circular running skin ridges on the tip of the index finger.

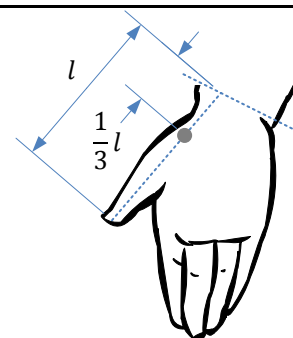


(19)/(20) Forefinger end joint The contact point is the outermost point of the end joint of the slightly bent forefinger.



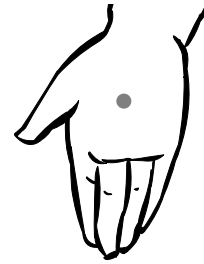
(21) Thenar eminence

The contact point lies on the line running along the fully outstretched thumb to the wrist. Its distance from the wrist is one-third of the line length.



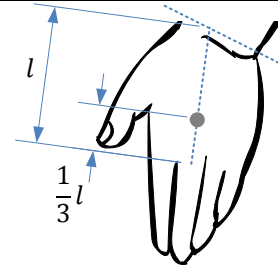
(22)/(23) Palm

The contact point is the deepest point in the center of the slightly closed hand.



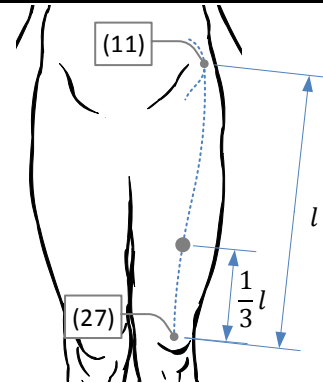
(24)/(25) Back of the hand

The contact point lies between the MCP of the middle finger to the wrist. The distance from the MCP is one-third of the total distance from the MCP to the wrist.



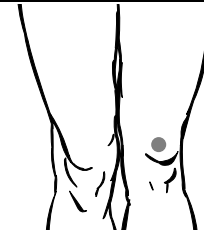
(26) Thigh muscle

The contact point is on the line running from (11) toward (27). Its proximal distance from (27) is one-third of the line's total length.



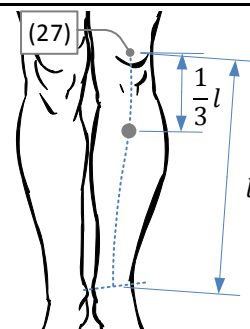
(27) Kneecap

The contact point is the outmost point in the center of the kneecap.



(28) Middle of shin

The contact point is on the line running from (27) toward the instep. Its distance from (27) is one-third of the line's total length.



(29) Calf muscle

The contact point is on the same level on the posterior side of (28).

